R. & M. No. 3693

R. & M. No. 3693

MINISTRY OF DEFENCE (PROCUREMENT EXECUTIVE)

AERONAUTICAL RESEARCH COUNCIL
REPORTS AND MEMORANDA

Pressure Measurements on a Model Delta Wing Undergoing Oscillatory Deformation

By N. C. LAMBOURNE, D. W. BRYER and J. F. M. MAYBREY

Aerodynamics Division, N.P.L., Teddington

LONDON: HER MAJESTY'S STATIONERY OFFICE

1972

PRICE £2·40 NET

Pressure Measurements on a Model Delta Wing Undergoing Oscillatory Deformation

By N. C. LAMBOURNE, D. W. BRYER and J. F. M. MAYBREY

Aerodynamics Division, N.P.L., Teddington

Reports and Memoranda No. 3693*
March, 1970

Summary.

Certain effects of leading-edge vortices on the surface pressures over a delta wing undergoing oscillatory deformation were investigated in a low-speed wind tunnel.

The model, consisting of a sharp-edged delta plate, could be deformed in a particular mode of chordwise bending over its forward portion only; the deformation could be applied either as a static condition or as a continuous variation in the form of a sinusoidal oscillation.

Surface pressures across the span were measured at two chordwise stations on the stationary part of the wing, the model being set throughout at a mean incidence of 5 degrees to ensure the presence of moderately strong vortices. The range of parameter variation was sufficient for the measurements to show the separate effects of frequency parameter and amplitude of deformation.

Spanwise distributions of Fourier harmonic components derived from the measured oscillatory pressure changes were examined in relation to the behaviour of the vortices; non-linearities are present in the relationship between pressure change and deformation, and analysis of the results indicates the magnitude of the harmonics above the fundamental that are present in the pressure variations at spanwise positions close beneath a vortex. The fundamental components of the pressure variations are compared with the results of calculations based on lifting-surface theory.

Within the limitations of the experiments (pressure measured only downstream of deformation) an empirical relationship involving a convective time-delay has been established between the unsteady pressures for an oscillatory deformation and the steady pressures for static deformations; the experimental conclusions are examined in relation to slender-wing theory, and more general implications of the results of the experiment are discussed.

LIST OF CONTENTS

*Replaces NPL Aero. Report 1314—A.R.C. 31 979.

LIST OF CONTENTS—*continued*

1. *Introduction.*

At least two new factors enter into the aeroelastic behaviour of slender delta wings as compared with the behaviour of high-aspect-ratio wings. Firstly, the predominant mode of wing deformation is chordwise bending; this involves changes of camber. Secondly, there are special effects arising from the leading-edge vortices which will be present above the wing for some values of incidence (Fig. 2). At the time the present work was started an investigation into the effects of oscillatory bending on the pressure distribution of a slender wing in the absence of leading-edge vortices was already being undertaken and has now been published (Ref. 1); the present investigation also involves chordwise bending but here the emphasis is on the special effects arising from the presence of vortices.

Some appreciation of the importance of the effects of leading-edge vortices can be obtained by a consideration of the upper-surface pressure distribution with a pronounced suction peak beneath the core of each vortex. Any change of incidence or deformation of the wing that causes a vortex to change its position relative to the wing is liable to lead to large non-linear changes in the local surface pressures. Another characteristic of vortex flow is the convection of vorticity above the upper surface of the wing. Under steady conditions vorticity is shed at a steady rate from the leading edges and is convected rearwards in the cores of the vortices. Under unsteady conditions, with incidence or deformation changing with time, the rate at which vorticity is shed varies so that there are variations in the vorticity convected over the wing which, in turn, lead to changes of local surface pressure. The experiments were intended to throw light on the non-linearities in the pressure variations and on the question of convected pressure changes.

When the model was designed there were no pressure transducers of suitable size and sensitivity that would function satisfactorily when attached to an oscillating body. This led to a choice of model with only the forward portion deformable, the pressures being measured only over the rigid rearward portion. The measurements consisted of spanwise pressure distributions at each of two chordwise positions so that any convective behaviour could be examined. For simplicity, both in constructing the flexible portion and in interpreting the pressure distributions, the model was designed to have a flat upper surface in the undeformed state.

2. *The Model Wing.*

The model delta wing was essentially a flat triangular-shaped plate having a 20 deg semi-apex angle and a centre-line chord of 1·22m [4 ft];* principal dimensions together with some details of construction are given in Figs. 3 and 4. The flat upper surface of the plate was constructed from a single sheet of Durestos, part of which was bonded to a rigid brass plate to form the rear stationary portion of the model. The forward and flexible portion of the Durestos sheet was built up to the same thickness as the rear portion by attaching balsa wood to the lower surface with its grain running normal to the surface to minimize resistance to bending. Sharp leading edges were provided by chamfering the lower surface at 20 deg normal to the edge.

The model was mounted on a rigid frame in the NPL 9 ft × 7 ft North Wind Tunnel (2·7m × 2·1m). It was provided with a spanwise axis at the mid-chord position and was held by an extendible strut at the rear for the adjustment of incidence; these features can be seen in Figs. 3 and 4. Also shown in Fig. 3 are details of the mechanism by which the cyclic distortion in longitudinal bending was imposed on the forward part of the model. Two forcing points on the centre-line of the wing were found to be necessary in order to avoid additional distortion due to aerodynamic loading; these were connected by a linkage designed to impose a mode corresponding to the steady mode of distortion obtained in 'still' air with the single forward forcing point. The linkage was driven by a forcing rod passing through the floor of the tunnel and connected to a reciprocating mechanism below. The amplitude of the motion could be changed by adjustment of the throw of an eccentric drive; the axial motion of the forcing rod was monitored by a linear-displacement transducer. The length of the forcing rod could be adjusted to set the mean position of the flexible portion of the wing. In the setting chosen as the undistorted condition, the upper surface was flat to within about 0·5 mm. With maximum deformation, measurements of surface

*Square brackets are used when the definitive value is in British, and not SI, units.

height along selected spanwise lines varied by no more than 0·5 mm.

'Wind-off' modes of deformation of the wing surface were obtained from measurements made at the approximate projected position in plan of the leading-edge vortices at a wing incidence of 5 deg. Measurements of the model deformation for vertical deflections of the driving rod of 2·54 mm [0·1 in] and 5·08 mm [0·2 in], were both found to give the mode of distortion that is shown in Fig. 13. It can be seen that, when deformed, the wing remains flat ahead of the forward forcing point.

Two spanwise stations on the fixed part of the wing at chordwise positions 0·583 c_0 and 0·833 c_0 were selected for pressure plotting and are denoted by ξ_1 and ξ_2 respectively.

Flush-diaphragm pressure transducers mounted in spanwise slots in the lower surface (Figs. 4 and 5) could be positioned to coincide with 0·4 mm holes drilled through the upper surface of the model, the surface holes being filled with wax when not in use; the volume of air over each transducer diaphragm was less than 60 mm^3. Alternative fittings were provided for connecting the surface holes to a tilting liquid manometer. For each of the two spanwise stations, 17 hole positions were chosen with close spacing in the regions of steep spanwise pressure gradient.

It will be clear, from the description above, that pressures could be measured only on the upper surface of the wing. Thus, pressures corresponding to a 'suction' surface were measured with the wing at positive incidence. Pressures corresponding to a 'pressure' surface were obtained in separate experiments with the wing mounted at a negative incidence.

3. *Instrumentation for Oscillatory Pressure Measurements.*

A block diagram of the instrumentation is given in Fig. 6. The pressure transducer (Type SE 76) which was a flush-diaphragm differential instrument was the only commercially-available type of suitable size and sensitivity; details of its performance and calibration have been given elsewhere.[2] Transducer output was recorded on a U.V. recorder. The sensitivity of the system was such that a 1 cm deflection of the trace represented 0·28 kN/m^2; the recording galvanometer limited the range of frequency response to 0 to 130 Hz.

Special transducer mountings (Fig. 5) were designed to minimize structural distortion to which the output was highly sensitive. To avoid transducer distortion arising from wind loads on the electrical and pressure leads it was necessary to shield these parts from the air stream, although this device contributed further to an already appreciable interference effect from the presence of the transducer when measuring pressures close to the leading edge.

It was found that the transducer was sensitive to small temperature changes, a change of 1 deg C being equivalent to a pressure change of 0·14 kN/m^2. To cope with possible variations of tunnel temperature, which could vary by as much as 5 deg C during a run, it was necessary to record with the pressure output, a signal from a thermocouple fixed to the case of the transducer.

To provide a signal proportional to the instantaneous deformation of the model and suitable for recording on the U.V. recorder, an SE 92 variable-reluctance linear-displacement transducer was fixed to the drive rod beneath the tunnel. A further record of the phase of the forcing motion was provided by pulses from photo-transistors responding to light interrupted by a toothed wheel mounted on the rotating drive shaft; these pulses were at intervals of 3·6, 18 and 36 deg of the cycle and were identifiable by different heights on the record.

The frequency of oscillation of the forcing mechanism, which was controlled manually, was indicated by feeding the 3·6 deg pulses to an integrating pulse counter. Timing lines at 0·1 second intervals were also recorded as a more accurate means of deducing frequency during subsequent analysis of the records; an example of a chart record is shown in Fig. 7 where the mean curve for the oscillating signal has been drawn by hand.

4. *Preliminary Observations and Measurements.*

To define a datum condition representing an effective zero incidence of the undeformed wing, a flow condition with attachment everywhere along the leading edges was sought. An examination of surface flow patterns using the paraffin and titanium dioxide technique showed that, for wind speeds of 30 m/s

[100 ft/sec] and 60 m/s [200 ft/sec], such a condition could not be reached, presumably owing to the effective camber of the non-symmetrical wing section and the interference effects of the model support. However, when the upper surface was set at an angle to the horizontal of $-1{\cdot}5$ deg, the flow patterns indicated that the flow was attached over most of the wing. Based on these observations, geometric angles of $+3{\cdot}5$ deg and $-6{\cdot}5$ deg were chosen to represent the effective incidences corresponding to an ideal flat plate at $+5$ deg and -5 deg respectively.

Preliminary observations of the surface flow using the same technique at the nominal incidence of $+5$ deg indicated that there was an area of the surface over which the boundary layer appeared to be laminar. To ensure a turbulent flow over the whole of the upper surface, carborundum grains were attached to the surface over a small triangular-shaped area near the apex, as can be seen in the oil flow photographs (Figs. 9 to 12).

The photographs of oil flow patterns on the wing at a mean incidence of $+5$ deg with the wing undeformed (Fig. 9); bent upwards ($\zeta_0 = +0{\cdot}0262$, Fig. 10) and bent downwards ($\zeta_0 = -0{\cdot}0262$, Fig. 11) were used to estimate the spanwise locations of the leading-edge vortices on the basis that their axes lay directly above the points of inflection in the oil flow lines. For the bent-up wing the vortex is inboard of its position when the wing is undeformed which in turn is inboard of the position when the wing is bent down. For the maximum bent-down condition the local incidence at the apex is close to zero and the pattern indicates that the vortices start from a position slightly downstream of the apex.

Flow patterns were also used to investigate possible interference effects on the upper surface flow arising from the disturbance caused by the pressure transducer attached to the underside of the wing. For the flow pattern shown in Fig. 12 a transducer was fixed in a position ($\eta = 0{\cdot}9$) close to the leading edge on the lower surface at Station ξ_1. From the flow pattern it is clear that a transducer at an outboard position at Station ξ_1 causes appreciable flow disturbance at Station ξ_2; for this reason no pressure transducer was attached at Station ξ_1 when measurements were being made at Station ξ_2. Although from the photograph there is little evidence of interference to the flow at Station ξ_1, it was subsequently shown by manometer readings that there was a measurable disturbance to the surface pressures but only outboard of the vortex.

5. *Steady Pressure Measurements.*

Initially, steady pressure distributions free of transducer interference were obtained from the manometer. These measurements were made at the nominal values of incidence ± 5 deg and five settings of wing distortion. They were then repeated with a dummy transducer to produce the interference that would be present when the oscillatory measurements were made. The two resulting sets of spanwise pressure distributions were used to provide corrections for interference on the pressures measured by the transducers.

As will be described in the next section, the steady pressure measurements with the manometer also provided a datum for the calibration of the instrumentation used to measure the oscillatory pressures.

6. *Recording and Analysis of Oscillatory Pressures.*

Measurements of oscillatory pressures were obtained at each of the spanwise positions by means of a single transducer shifted from one position to another in turn. Because of the need for frequent recalibration of the transducer system and to correct for the effects of temperature changes, the following routine was adopted. As illustrated schematically in Fig. 8, a chart record of a tunnel run consisted of traces from the pressure transducer and its associated thermocouple firstly for the steady undeformed wing, next for a quasi-steady variation consisting of a very slow oscillation ($f \simeq 0{\cdot}2\ Hz$), and then for each of the higher frequencies used. Between the oscillations at each frequency the wing was brought rapidly to rest in the undeformed condition and the pressure recorded by short traces. Brief records were then made for the wing held stationary at the extreme amplitudes.

The traces *a*, *b*, *c* etc., for the undeformed wing could be related to the pressures already accurately measured by the manometer. The oscillatory pressure traces could thus be corrected for temperature changes by means of a previously determined linear relationship between temperature and transducer

output. Similarly, the traces D_1 and D_2 could be related to the steady pressure changes due to deformation already measured by a manometer so that they provided an immediate check on the sensitivity of the transducer. This routine was repeated for each of the pressure holes in turn.

In the sample portion of a recorded trace shown in Fig. 7, the higher frequency fluctuations apparent in the pressure record are attributed to the turbulent boundary layer. For the analysis of a record, a smooth pencil line was drawn through the trace and the displacement of this line from a fixed datum was measured at each 18 deg interval of the phase angle ϕ (*see* equation (2) in Section 7.1) over at least four consecutive cycles.

For pressure holes near to the leading edge, corrections were made for the interference arising from the blockage effect of the transducer below the wing. This was done by subtracting from the measured pressures for each value of ϕ the difference between 'interference free' and 'with interference' values obtained under steady conditions, using the manometer as already described in Section 5.

After converting the measured pressures to non-dimensional values of C_p and obtaining mean values over the four cycles, spanwise distributions of C_p were plotted and, for each of the 20 values of ϕ, smoothed curves were drawn. From these, interpolated values of C_p for 42 positions across the span for each of the 20 values of ϕ, together with the measurements of the pressure appropriate to the 'pressure' surface obtained in separate experiments were read off. Subsequently these were processed on a KDF 9 computer to give Fourier coefficients of ΔC_p, the non-dimensional difference in pressure between the 'suction' and 'pressure' surfaces, and the related phase angles for each spanwise position. Spanwise sectional lift coefficients were calculated in the same programme.

In the harmonic analysis of the results, components were calculated up to the 6th order but those above the 3rd order were always found to be too small to be of significance.

Since the pressures for a very slow oscillation are related uniquely to displacement, the harmonic components obtained for one amplitude can be used to deduce harmonic coefficients for a quasi-steady variation of smaller amplitude.

7. *Presentation of Results.*

7.1. *Nomenclature.*

The co-ordinate system is shown in Fig. 1. A position on the wing surface is specified by the non-dimensional co-ordinates

$$\xi = x/c_0, \quad c_0 \text{ being the centre-line chord,}$$

$$\eta = y/s \ , \quad s \text{ being the local semi-span.}$$

The *upward* displacement of a spanwise section of the distorting portion of the wing is

$$z = z_0 F(\xi) \tag{1}$$

where z_0 is the displacement of the leading apex and $F(\xi)$ the mode of deformation referred to the apex so that $F(o)=1$. Under cyclic conditions the apex displacement is related to an angular co-ordinate ϕ, representing a rotation in the forcing mechanism, and an amplitude $\bar{z}_0$ by the equation

$$z_0 = \bar{z}_0 \cos \phi \, , \tag{2}$$

which serves for a quasi-steady variation. For an oscillation of frequency ω, $\phi = \omega t$ and the apex deflection is then

$$z_0 = \bar{z}_0 \cos \omega t \, . \tag{3}$$

The motion of a general point on the deforming portion is

$$z=\bar{z}\cos\omega t=\bar{z}_0 F(\xi)\cos\omega t \tag{4}$$

for an oscillatory condition, and

$$z=\bar{z}\cos\phi\ =\bar{z}_0 F(\xi)\cos\phi \tag{5}$$

for a quasi-steady variation.

The measured surface pressures are expressed as non-dimensional coefficients

$$C_p=(p-p_0)/\tfrac{1}{2}\rho V^2, \tag{6}$$

where p_0 is the pressure in the undisturbed stream. The resultant loading from the two surfaces of the wing is

$$\Delta C_p=(p_l-p_u)/\tfrac{1}{2}\rho V^2=C_{p_l}-C_{p_u} \tag{7}$$

which when positive corresponds to upward lift.

For an oscillation defined by equation (3) the cyclic variation in the loading at each position on the wing can be expressed as a Fourier series in either of the following alternative forms:—

$$\Delta C_p=R_0+R_1\cos(\omega t-\varepsilon_1)+R_2\cos(2\omega t-\varepsilon_2)+\ldots \tag{8}$$

or

$$\Delta C_p=A_0+A_1\cos\omega t+A_2\cos 2\omega t+\ldots$$
$$+B_1\sin\omega t+B_2\sin 2\omega t+\ldots, \tag{9}$$

where

$$\left.\begin{aligned} A_0\equiv R_0,\ A_1\equiv R_1\cos\varepsilon_1,\ A_2\equiv R_2\cos\varepsilon_2 \\ B_1\equiv R_1\sin\varepsilon_1,\ B_2\equiv R_2\sin\varepsilon_2 \end{aligned}\right\}.$$

For a quasi-steady variation defined by equation (2) the pressure distribution must of necessity be symmetric about $\phi=0$ and $\phi=\pi$. Thus, only the cosine terms appear in the Fourier series and we have

$$\Delta C_p=S_0+S_1\cos\phi+S_2\cos 2\phi+\ldots, \tag{10}$$

where the coefficients S_n correspond to the coefficients A_n in equation (9) and $|S_n|$ is the quasi-steady equivalent of R_n in equation (8).

A measure of the harmonic distortion in the cyclic variation of pressure is afforded by

$$H=\left[\sum_{n=2}^{\infty}(A_n^2+B_n^2)\right]^{\frac{1}{2}}\equiv\left[\sum_{n=2}^{\infty}R_n^2\right]^{\frac{1}{2}} \tag{11}$$

or, for a quasi-steady variation, by

$$H=\left[\sum_{n=2}^{\infty}S_n^2\right]^{\frac{1}{2}}. \tag{12}$$

The fundamental components of pressure in phase and in quadrature with the wing motion are normalized with respect to frequency and amplitude of apex deflection, thus

$$a_1 = \frac{A_1}{\bar{\zeta}_0} \tag{13}$$

$$b_1 = \frac{B_1}{\nu.\bar{\zeta}_0} \tag{14}$$

where the non-dimensional amplitude

$$\bar{\zeta}_0 = \bar{z}_0/c_0$$

and the frequency parameter

$$\nu = \omega c_0/V.$$

7.2. *Parametric variations.*

For a delta wing of particular shape oscillating in the given mode of deformation about a constant mean incidence, the surface pressures are expected to depend on the following quantities:—

$$c_0, \bar{z}_0, x, y, \rho, \mu, V \text{ and } \omega .$$

Dimensional analysis then shows that the non-dimensional pressure coefficient ΔC_p will be dependent on the following non-dimensional parameters:—

Reynolds number	$Re = \rho V c_0/\mu$,
Frequency parameter	$\nu = \omega c_0/V$,
Deformation amplitude	$\bar{\zeta}_0 = \bar{z}_0/c_0$,
Chordwise position	$\xi = x/c_0$
Spanwise position	$\eta = y/s$.

Thus the general form of the cyclic pressure variation can be written in terms of Fourier components as follows:—

$$\Delta C_p = \sum_{n=0}^{\infty} R_n \left\{ \eta, \xi, \bar{\zeta}_0, \nu, Re \right\} \cos \left[n\omega t - \varepsilon_n \left\{ \eta, \xi, \bar{\zeta}_0, \nu, Re \right\} \right]. \tag{15}$$

The aim of the experimental programme was to throw light on the functional dependencies in the right-hand side of the above equation.

Measurements of spanwise pressure distribution over the region $0 < \eta < 1$ were made at each of the two chordwise positions

Station ξ_1 (=0·583)

Station ξ_2 (=0·833),

for each of two amplitudes of deformation

'small amplitude' $\bar{\zeta}_0 = 0{\cdot}0131$

'large amplitude' $\bar{\zeta}_0 = 0{\cdot}0262$.

Variation of frequency parameter was obtained by changes of frequency and wind speed; a change of wind speed provided a change of Reynolds number. The following table shows the combinations used during the measurements.

V	$f=\frac{\omega}{2\pi}$	ν	Re
30 m/s	0 *Hz*	0	$2{\cdot}56\times10^6$
,,	2	0·5	,,
,,	4	1·0	,,
60 m/s	0	0	$5{\cdot}11\times10^6$
,,	4	0·5	,,

7.3. *Mode of deformation and local incidence.*

All the measurements refer to the wing with a nominal incidence, $\alpha_0 = 5$ deg. The mode of deformation, as defined by equation (1) is given in Fig. 13.

The local incidence, or slope of the wing, is

$$\alpha_s(\xi) \simeq \alpha_0 - dz/dx = \alpha_0 - (\zeta_0)\, F'(\xi)\,. \tag{16}$$

Distributions of this quantity for steady upward and downward deformations are shown in Fig. 14.

7.4. *Results and analysis.*

Values of ΔC_p were obtained for the parametric combinations given in the following table:—

Parametric condition		
Amplitude $\bar{\zeta}_0 = z_0/c_0$	Frequency ν	Reynolds number $Re \times 10^{-6}$
'Large amplitude' 0·0262	0	2·56
,,	0·5	,,
,,	1·0	,,
,,	0	5·11
,,	0·5	,,
'Small amplitude' 0·0131	0	2·56
,,	0·5	,,
,,	1·0	,,
,,	0	5·11
,,	0·5	,,

Comprehensive tabulated results, if required, are available from another document*.

However, for the purpose of the discussion in Section 8 many of the results are displayed graphically. In order to bring out salient points, the following forms of plotting are used:—

(i) Pressure at a given position as a function of wing deformation for steady and unsteady conditions (Fig. 15)
(ii) Spanwise pressure distributions for a static deformation (e.g. Fig. 17)
(iii) Instantaneous spanwise pressure distributions for oscillatory conditions (e.g. Fig. 31)
(iv) Spanwise distributions of harmonic components of the pressure for oscillatory conditions and quasi-steady variation (e.g. Figs. 19 and 20)
(v) Polar plots of amplitude and phase of harmonic pressure components (e.g. Fig. 29).

8. *Discussion.*

8.1. *Steady flow over a delta wing at incidence.*

Before discussing the results of the pressure measurements, it may be helpful to review the principal features of the flow over the upper surface of a delta wing under steady conditions.

The flow over an uncambered slender delta wing with sharp edges separates from the leading edges at quite low values of incidence. The vortex layers so formed roll up to give two vortices lying above the upper surface and extending into the wake as illustrated schematically in Fig. 2. The vortex flow leads to the characteristic surface flow pattern shown by the photograph of Fig. 9. More detailed examination of the flow pattern reveals the existence of an attachment line inboard of the vortex and a secondary separation line slightly outboard of the vortex; between the latter and the leading edge one or more subsidiary vortices may be present. The spanwise pressure distribution shows that, for a flat surface, the pressure between the attachment lines is approximately constant, whilst a suction peak exists beneath each vortex. These features can be seen in the spanwise pressure distributions shown in Figs. 16 and 17.

8.2. *Flow changes due to steady deformation.*

Figs. 16 and 17 show the upper and lower surface pressure distributions for the undeflected wing and for maximum upward and downward deflections corresponding to the largest amplitude of oscillation used in the measurements. Lower-surface pressure changes due to deformation are negligible, and the features in the cyclic variations of the resultant pressure ΔC_p can be attributed solely to the suction surface. The pressure changes occurring inboard of the attachment line appear consistent with attached flow and the variation in forward camber. Those occurring outboard of the attachment line seem to be determined by the displacement of the vortex resulting from the deformation; there are appreciable changes in the height and spanwise position of the suction peak and these can be related to the changes in oil pattern shown by Figs. 9 to 11. When the forward part of the wing is deflected upwards (Fig. 10), the vortex at Stations ξ_1 and ξ_2 moves inboard; so also does the suction peak, but its magnitude is reduced. With downward deflection of the wing (Fig. 11), the vortex and suction peak move outboard.

These changes can be partly explained in the following manner by a consideration of the effects of wing incidence on vortex strength and position. For an undeformed wing at incidence, it is known that with increasing incidence the strength of the vortex increases and its position moves inboard and higher above the wing. Thus, with upward distortion, which increases the incidence of the forward part of the wing, the strength of the vortex would be greater but its height above the wing would also be increased; from the surface pressure measurements over the stationary part of the wing it is apparent that the effect on the suction peak of increasing the height of the vortex outweighs the effect of an increase in the vortex strength. For a downward distortion, a vortex of reduced strength is now closer to the surface of the wing and produces a peak whose magnitude appears to be sensitive to wind speed. This sensitivity to wind speed is thought to be the result of the change in Reynolds number altering the details of the vortex flow at the apex. With full downward deformation, when the local incidence at the apex is less than

*NPL Aero. Report 1314.

0·5 deg, the point of origin of the vortices is no longer at the leading apex; Fig. 11 shows that the vortices originate near the position $\xi=0{\cdot}1$ at 30 m/s when the wing is deflected fully downwards. No similar flow pattern is available for 60 m/s, but it is possible that the vortex origin would then move forward with the vortex adhering somewhat more closely to the wing surface to give greater suction.

From the surface flow patterns, the attachment lines at Station ξ_1 are estimated to be as follows:—

Wing deformation	ζ_0	η (attachment)
Max. upwards	+0·0262	0·51
Undeformed	0	0·63
Max. downwards	−0·0262	0·72

The position of the attachment line for each deformation condition is marked on Figs. 16 and 17 and it will be seen that there is an approximate correlation between this position and that of the minimum suction in the pressure distribution. This is only to be expected since the attachment line is somewhat analoguous to a stagnation line. Broadly speaking, the effects of vortex flow can be regarded as being restricted to the region outboard of the attachment line.

8.3. *Harmonic components of the cyclic pressure variation.*

It will be most convenient to discuss the distribution of ΔC_p for a quasi-steady variation before dealing with the more general oscillatory condition. The Fourier harmonic analysis then includes only the cosine components as in equation (10); the spanwise distributions of S_0, S_1, S_2 etc., are shown in Fig. 18. We note that the mean level S_0 resembles, as would be expected, the pressure distribution for the steady undeformed wing, except that the width of the S_0 peak is rather greater than the steady suction peak of Fig. 17. With regard to the spanwise distributions of the other components, we can relate the salient features to the pressure distributions for steady deformation of the wing as shown in Fig. 17 and to the variations of pressure at fixed points as shown in Fig. 15. For this purpose we consider the types of pressure variation that can be deduced from Fig. 17 for a quasi-steady variation between maximum downward and maximum upward deformation; for the purpose of discussion, portions of the semi-span are denoted by $\gamma, \delta, \delta_1, \delta_2$, etc., as indicated in Fig. 17.

Over region γ, which extends over approximately the inner half span, it is seen that the suction ΔC_p, decreases with increasing upward deformation, and that the variation is approximately linear, as in Fig. 15(a). Accordingly, Fig. 18 shows that over this portion of the span the only harmonic component of significance is the fundamental component S_1, and that the sign of this is negative. Over the outer region δ, the movement of the suction peak resulting from wing deformation leads to non-linear variations of the pressure as shown in the other examples of Fig. 15, and correspondingly to the presence of appreciable harmonic components of the second and higher orders, as shown in Fig. 18. It may be noted that the region where the higher harmonics are significant correlates approximately with the region outboard of the extreme inboard position of the attachment line. That is, the higher harmonics only occur over the region directly influenced by the vortex. For all the conditions examined in the experiments, the peak values of the harmonic components decrease with increasing order, those for the 4th and higher orders appearing too small to be of importance, for which reason they are not included in the diagrams. Each of the harmonic components shows alternations of sign over the outboard half of the span. It can be deduced from Fig. 17 that over a region δ_2 in the neighbourhood of $\eta=0{\cdot}7$ the predominant variation is ΔC_p increasing with z_0, as in Fig. 15(b); thus this region corresponds to a maximum in the fundamental component, with suction increasing with upward displacement (i.e. $S_1>0$). Over region δ_4, outboard of approximately $\eta=0{\cdot}83$, the predominant variation is ΔC_p decreasing with z_0, as in Fig. 15(d); this corresponds to a large negative value for S_1. Between δ_2 and δ_4 we have region δ_3 corresponding to the position of the suction peak for the undeformed wing. During one cycle of oscillation the peak passes

twice over a point in this region, as in Fig. 15(c); this leads to a cyclic pressure variation which consists mainly of the second harmonic as shown in Fig. 18. From Fig. 17 we can identify another region of the span, δ_1 where the suction for the undeformed wing is lower than that for either upward or downward deformation. Thus this region experiences a minimum suction twice during a cycle and, as for δ_3, the cyclic variation contains a large proportion of second harmonic.

Turning now from the quasi-steady variation, we consider the main features of the pressure variations for an oscillatory condition. An oscillation at non-zero frequency leads to phase differences between pressure and deformation and thus to closed loops in the variation of ΔC_p and z_0 as seen in the full-line curves of Fig. 15. However, the spanwise distributions of the amplitudes of the harmonic components retain the same general form as can be seen by a comparison of, say, Figs. 19 and 20 for Station ξ_1 and Figs. 21 and 22 for Station ξ_2.

Examples of the spanwise distributions of the Fourier coefficients A_n and B_n corresponding to the first three harmonics are shown in Figs. 25 to 28. For Station ξ_1 the effect of frequency on the coefficients A_n can be seen by a comparison of the curves of Fig. 18 with the relevant curves of Figs. 25, 27 and 28. In general, the peaks in the distributions are somewhat reduced for the oscillation with non-zero frequency. It will be noticed that in many cases the spanwise fluctuations in a component B_n are similar in form to the fluctuations in the corresponding component A_n.

The spanwise variations of phase angles are most conveniently displayed by plotting (R_n, ε_n), the amplitude and associated phase angle of a harmonic component, on a polar diagram for a series of spanwise positions. Figs. 29 and 30 show the first three harmonic components through the range $0<\eta<1{\cdot}0$ plotted in this way for Stations ξ_1 and ξ_2 respectively. In each case the cluster of points is elongated about a line passing through the origin, thus indicating a tendency for the pressure variations at points across the span to be in phase (or anti-phase) with one another; this tendency is less strong for the higher harmonics. Lines have been drawn to show estimated mean values of phase angles ε (or $\pi+\varepsilon$) across the span which are thus weighted in favour of the modulus of the component. It will be noticed that these mean phase angles associated with the harmonic components increase approximately as the order of the harmonic; that is, the measured phase angles tend to be in accord with the relationship,

$$\varepsilon_n' = k_1 n (\text{radians}), \tag{17}$$

where $\varepsilon_n' = \varepsilon_n$ or $\varepsilon_n - \pi$, and k_1 is a constant.

This point will be discussed in more detail in Section 8.5.

8.4. *Effect of change of wind speed.*

For steady conditions, a change of wind speed could be expected to affect the pressures for two possible reasons (a) because the resultant change in Reynolds number leads to a change in the type of flow, and (b) because a change in aerodynamic loading alters the mode of deformation of the wing.

To determine any sensitivity of the pressure measurements to a change of wind speed, results obtained for speeds of 30 m/s were compared with those for 60 m/s for Stations ξ_1 and ξ_2. A comparison for steady conditions is afforded by Figs. 16 and 17 from which it is seen that there is general agreement on the form of the pressure distributions both for the deformed and the undeformed wing, but that there are differences in the positions and heights of the suction peaks. As already mentioned in Section 8.2, it is thought that the appreciable change in height of the peaks when the apex is in the extreme downward position may arise from small changes in the manner in which the flow separates from the leading-edge near the apex.

For an oscillatory condition the effect of wind speed can only be seen by comparing results for the same value of frequency parameter. That is, for $\nu=0{\cdot}5$, results for 2 Hz and 30 m/s are comparable with those for 4 Hz and 60 m/s. Examples of the spanwise distributions of Fourier coefficient R_n for the two wind speeds from which such comparison can be made are shown in Figs. 23 and 24. Although there are some differences of detail between results for the two wind speeds, both sets exhibit the same general features.

The subsequent discussion relates only to results obtained at a wind speed of 30 m/s as these alone include measurements at both the non zero values of frequency parameter.

8.5. *Influence of frequency.*

It has already been noted with reference to Figs. 19 to 22, that there is a similarity between the spanwise distributions of the amplitudes of the harmonic components of the pressure variations for a quasi-steady variation and for an oscillatory condition. Such similarity is found for all the comparisons that can be made between quasi-steady and oscillatory conditions, and this leads to the conclusion that the amplitude of each Fourier component for an oscillation is approximately the same as that of the corresponding component for a quasi-steady variation, that is $R_0 \simeq |S_0|$, $R_1 \simeq |S_1|$, $R_2 \simeq |S_2|$, etc.

In the following table, mean values of phase angle across the span have been deduced numerically for each set of experimental conditions whilst, on the basis that a relationship $\varepsilon'_n = k_1 n$ is appropriate, mean values of k_1 weighted in favour of the lowest harmonic and the largest amplitude of deformation are also shown.

Phase angles (in radians).

Columns (*l*) and (*s*) refer respectively to the large and the small amplitude of oscillation.

Order of Harmonic Components	Station $\xi = \xi_1 = 0{\cdot}583$		Station $\xi = \xi_2 = 0{\cdot}833$	
	$\nu = 0{\cdot}5$	$\nu = 1{\cdot}0$	$\nu = 0{\cdot}5$	$\nu = 1{\cdot}0$
	(*l*) (*s*)	(*l*) (*s*)	(*l*) (*s*)	(*l*) (*s*)
$n=1$	0·30, 0·28	0·59, 0·60	0·42, 0·39	0·84, 0·84
$n=2$	0·58, 0·59	1·19, 1·23	0·85, 0·87	1·68, 1·68
$n=3$	0·94, 1·00	1·91, —	— —	— —
Weighted mean phase $\varepsilon'_n \equiv k_1 n$	0·29 n	0·58 n	0·41 n	0·84 n
$k_1/\nu\xi$	1·00	1·00	0·99	1·01

From the tabulated values it is evident that a phase angle for the higher frequency ($\nu = 1{\cdot}0$) is approximately twice that for the lower frequency ($\nu = 0{\cdot}5$).

Thus with regard to the influence of frequency, we are led to the conclusion that the amplitudes R_n of the harmonic components are approximately independent of frequency whilst the associated phase angles are related to frequency and harmonic order by an approximate relation

$$\varepsilon'_n \simeq k_2 n\nu . \tag{18}$$

8.6. *Effect of change of chordwise position.*

The general features of the spanwise distributions of the harmonic coefficients for Station ξ_2 are similar to those already described for Station ξ_1, but the amplitudes of the pressure variations are less (as can be seen from a comparison of Figs. 20 and 22) and, for oscillatory conditions, the phase angles associated with the Fourier components are larger (as can be seen from a comparison of Figs. 29 and 30). From the table of Section 8.5, it is seen that phase angle is approximately proportional to ξ. This agrees with the results obtained with a delta wing performing sinusoidal plunging motion[3], where it was found that the timewise variations both of the pressures measured at points along a ray through the leading apex (η = constant) and of the height of the vortex involved phase angles with respect to the plunging motion that increased linearly with distance from the apex. The present measurements lead to the further conclusion that the phase angles, when expressed in radians, are approximately equal to $n\nu\xi$. Now any

phase angle ε'_n, that is associated with a frequency $n\omega$, can be related to a time delay $\tau = \varepsilon'_n/n\omega$ which, when normalized with reference to the free-stream velocity and chordwise distance from the apex, becomes a non-dimensional time delay

$$\tau V/x = \varepsilon'_n V/n\omega x = \varepsilon'_n/nv\xi = k_1/v\xi \,. \tag{19}$$

None of the values of $(\tau V/x)$ shown in the table departs significantly from unity. It will be noted that the value of τ deduced from the experiments is the same as the free-stream convection time from the apex to the pressure-measuring station. This point will be discussed later in Section 10.

8.7. *Empirical relationship between steady and oscillatory loadings.*

Based on the foregoing observations, it is possible to put forward an expression which relates the oscillatory load distributions to those for a quasi-steady variation. It is convenient to start with the completely general description of the cyclic variation of spanwise pressure distribution for fixed amplitude of deformation,

$$\Delta C_p(\eta, \xi, v) = R_0(\eta, \xi, v) + R_1(\eta, \xi, v) \cos [\omega t - \varepsilon_1(\eta, \xi, v)] + R_2(\eta, \xi, v) \cos [2\omega t - \varepsilon_2(\eta, \xi, v)] + \ldots \tag{20}$$

Now the experimental results already discussed suggest that with some degree of approximation, the following statements hold:—

(i) Each $R_n(\eta, \xi, v)$ is independent of frequency and can be replaced by $|S_n(\eta, \xi)|$.

(ii) Each $\varepsilon_n(\eta, \xi, v)$ is independent of η and thus can be replaced by $\varepsilon_n(\xi, v)$.

(iii) Each $\varepsilon_n(\xi, v)$ is proportional to the product of harmonic order and frequency so that

$$\varepsilon_n(\xi, v) = \tau n\omega \text{ or } \tau n\omega + \pi \,,$$

τ being a time delay.

(iv) The time delay τ is proportional to the chordwise distance and can be equated to the convective time from the apex, i.e.

$$\tau = \xi c_0/V.$$

Thus from statements (i), (ii) and (iii) above we may write

$$\Delta C_p(\eta, \xi, v) = S_0(\eta, \xi) + S_1(\eta, \xi) \cos [\omega(t - \tau)] + S_2(\eta, \xi) \cos [2\omega(t - \tau)] + \ldots \tag{21}$$

That is, the pressure distributions for an oscillatory condition are the same as those for a quasi-steady variation but with a time delay with respect to the deformation. Statement (iv) gives the dependency of $\omega\tau$ on frequency parameter and chordwise co-ordinate, so that finally we have

$$\Delta C_p(\eta, \xi, v) = S_0(\eta, \xi) + S_1(\eta, \xi) \cos (\omega t - v\xi) + S_2(\eta, \xi) \cos 2(\omega t - v\xi) + \ldots \tag{22}$$

That is, equation (22) gives the oscillatory spanwise pressure distribution in terms of the harmonic components for a quasi-steady variation, the frequency parameter and chordwise co-ordinate. Equating the separate harmonic components for oscillatory conditions with those for a quasi-steady variation we have for Station ξ,

$$
\left.\begin{aligned}
&A_0(\eta)=S_0(\eta) \\
&A_1(\eta)=S_1(\eta)\cos\nu\xi \quad , \quad B_1(\eta)=S_1(\eta)\sin\nu\xi \\
&A_2(\eta)=S_2(\eta)\cos 2\nu\xi \, , \quad B_2(\eta)=S_2(\eta)\sin 2\nu\xi
\end{aligned}\right\} . \tag{23}
$$

As a test of the effectiveness of these relationships, values of the right-hand sides of equations (23) have been calculated for $\nu=1{\cdot}0$ at Stations ξ_1 and ξ_2, and these are compared in Figs. 25 to 28 with values of the left-hand sides deduced from the oscillatory measurements. The largest discrepancy occurs for the third harmonic component at Station ξ_1 (Fig. 28). Apart from this and some differences in the region close to the side edge,* there is excellent agreement between the measured and calculated distributions.

A series of instantaneous pressure distributions at ξ_2 and for $\nu=1{\cdot}0$ at each of the cyclic times $\omega t=0$, $\pi/2, \pi$ and $3\pi/2$, have been deduced from equation (22) and these are compared with the measured instantaneous pressure distributions in Fig. 31. Also shown in this diagram, for the purpose of illustrating the time displacement in the pressures, are the measured pressure distributions for the same deformations of a stationary wing; these are identical with values obtained from equation (22) with $\nu\xi$ equated to zero.

Stated in another way, the conclusion from the experimental results is that the measured instantaneous spanwise distribution of pressure for position ξ' at time t' during an oscillation corresponding to frequency parameter ν, matches the steady pressure distribution at ξ' for a steady deformation of the wing given by

$$
z=\bar{z}_0 F(\xi)\cos(\omega t'-\nu\xi') . \tag{24}
$$

This conclusion will be further discussed in Section 10.

8.8. *Fundamental Fourier components.*

The fundamental components of the cyclic variation in loading are of special interest because these are the only ones that would be considered in a linear analysis. Normalized with respect to amplitude of deformation and frequency, these components are from equation (9),

$$
a_1=A_1/\bar{\zeta}_0 \; =(R_1/\bar{\zeta}_0)\cos\varepsilon_1 , \tag{25}
$$

$$
b_1=B_1/\nu\bar{\zeta}_0=(R_1/\nu\bar{\zeta}_0)\sin\varepsilon_1 . \tag{26}
$$

These quantities correspond respectively to the in phase and in quadrature derivatives of the loading. From Figs. 32 and 35, which show spanwise distributions of a_1 it is seen that the peaks are reduced both by an increase of frequency and by an increase of amplitude. Figs. 33 and 35 show that the spanwise distributions of b_1 are mostly insensitive to frequency although the peak values decrease with increasing amplitude. The results thus indicate that the fundamental pressure components exhibit amplitude non-linearities over those areas directly influenced by the vortex flow, the distributions becoming less peaky with increasing amplitude. The variations with frequency are consistent with the general conclusions of Section 8.5 and 8.6, for if $\varepsilon_1=\nu\xi$ we have

$$
a_1=\frac{R_1\cos\nu\xi}{\bar{\zeta}_0}\simeq\frac{R_1}{\bar{\zeta}_0}\left[1-\frac{(\nu\xi)^2}{2}\right], \tag{27}
$$

$$
b_1=\frac{R_1\sin\nu\xi}{\nu\bar{\zeta}_0}\simeq\frac{R_1\xi}{\bar{\zeta}_0}\left[1-\frac{(\nu\xi)^2}{6}\right]. \tag{28}
$$

Thus, if as previously noted R_1 is insensitive to frequency, the magnitudes of a_1 and b_1 will both decrease

* The term 'side edge' seems more appropriate than 'leading edge' when discussing spanwise sections.

with frequency, but b_1 will be affected less than a_1.

Measurements for oscillatory conditions were made for only two amplitudes of deformation, but measurements for steady conditions were made for a range of deformation; thus the harmonic components corresponding to a quasi-steady variation can be deduced for any amplitude that falls within the range of deformation covered. The spanwise distributions of $|S_1|/\bar{\zeta}_0$ that are plotted in Fig. 36 relate to a series of amplitudes and show that in the region directly under the influence of the vortex flow, the value of this quantity decreases with amplitude. Since the Fourier components for a quasi-steady variation and for an oscillatory condition are similar, the curves of Fig. 36 can also be regarded as representing the behaviour of $R_1/\bar{\zeta}_0$ with amplitude of deformation.

8.9. *Influence of amplitude on harmonic distortion.*

The quantity H in equation (11) is a measure of the total magnitude of the components above the fundamental that are present in the loading and, by comparison with the amplitude of the fundamental R_1, it represents the harmonic distortion. Fig. 38 shows a comparison between the spanwise distributions of H and R_1 for the large amplitude of oscillation and highest value of frequency. As already mentioned in Section 8.3, the harmonic distortion is large in the region directly beneath the vortex and small over the region inboard of the attachment line. The corresponding diagram for a quasi-steady variation of the same amplitude would be almost identical with Fig. 38, whilst by comparison, Fig. 39 for a quasi-steady variation of much smaller amplitude shows a considerable reduction in harmonic distortion. Since $R_n \simeq |S_n|$ the general influence of varying amplitude can be obtained by an examination of its effects on the harmonic components for quasi-steady variations. Fig. 37 shows, for a range of deformation amplitudes, the spanwise distribution of $H/\bar{\zeta}_0$ the normalized harmonic distortion. Whilst Fig. 36 shows $|S_1|/\bar{\zeta}_0$ decreasing with increasing amplitude, there is a tendency for $H/\bar{\zeta}_0$ to increase with deformation. The spanwise region over which there is appreciable harmonic distortion does not vary much with amplitude of deformation and, as previously mentioned, this region coincides approximately with the part of the wing surface between the flow attachment line and the side edge. Within this region the ratio of the higher harmonic content to the fundamental generally increases with increase of wing deformation.

8.10. *Spanwise integration of pressure.*

An attempt was made to deduce values of the cyclic variation in the spanwise sectional lift coefficient,

$$C_L(\xi) = \int_0^1 \Delta C_p(\xi, \eta)\, d\eta\,, \tag{29}$$

from the measured pressure distributions. Graphical integration of the curves of Fig. 16 gives the following values:—

ζ_0	$C_L(\xi_1)$ (Station ξ_1)
−0·0262	0·198
0	0·203
+0·0262	0·206

It will be noticed that the change in the sectional lift due to deformation is quite small in comparison with the total sectional lift, thus showing the need for accuracy in the integrations. Further evidence of the care needed, when using the measured pressure distributions to obtain reliable values of the changes of sectional lift, comes from the following alternative approach.

For the steady deformations given by $z = \bar{z}_0 \cos \phi$, we have

$$C_L(\xi) = \int_0^1 \Lambda C_p \, d\eta = L_0 + L_1 \cos \phi + L_2 \cos 2\phi + \ldots \tag{30}$$

where

$$L_n = \int_0^1 S_n \, d\eta \, .$$

Within the scope of a linear approximation, $L_1/\bar{\zeta}_0$ would have the form of a derivative whilst L_2, L_3 etc., correspond to the harmonic distortion (or non-linearities) in the variation of sectional lift. Now with regard to the integrals L_1, L_2 and L_3, inspection of the particular example in Fig. 18 suggests that the fluctuations of S_1, S_2 and S_3 lead to positive and negative contributions to the integrals which tend to cancel. The situation is more readily appreciated from Fig. 40 which, by showing part-span integrals $\int_0^{\eta_1} S_n \, d\eta$ plotted as functions of η_1, emphasizes the sensitivity of the values of L_1, and L_2 and L_3 to contributions from points close to the side edge, where the uncertainties of the pressure measurements are known to be greatest.

9. *Comparison with Lifting-Surface Calculations.*

It has already been shown in Ref. 1 that, for a delta wing at zero incidence without vortex flow, calculations based on lifting-surface theory can provide reasonable agreement with measurements of unsteady pressure distributions resulting from an oscillatory deformation. Since in the usual lifting-surface theory the flow is assumed to remain attached over the surface of the wing, calculations based on this theory would certainly not provide the kind of pressure distributions observed with vortex flow. Nevertheless, it is of some interest to make comparison between this theory and the results of the present measurements to see whether agreement exists for those areas of the wing surface not directly under the influence of vortex flow. The assumption of linearity between pressure and deformation inherent in the theory, means that the calculations yield only sinusoidal pressures in response to the sinusoidal deformation; thus comparisons can only be made with the fundamental Fourier component of the measured pressure variations. Calculations for small frequency have been made by the method of Garner and Fox[9]. The results for the in-phase component a_1 are shown in Fig. 32 where it is seen that there is some measure of agreement regarding the order of magnitude of the coefficient over the inboard region of attached flow. The corresponding calculated value of the in-quadrature component b_1 approximately $-0{\cdot}1$ over the whole of the span except for the singularity at the side edge; this magnitude is small in comparison with the fluctuations shown in Fig. 33, but the value is of the same order as the measurements over the inboard region of the span.

Theoretical values of the part-span in-phase loading corresponding to the experimental $\int_0^{\eta_1} S_1 \, d\eta$ have also been calculated. Fig. 40 shows that there are considerable differences between the theoretical and measured values even over the inboard region which is not directly under the influence of the vortices.

Although the lifting-surface calculations included only a small number of collocation points over the deforming portion of the wing, they are sufficient to show the large differences between the theoretical and measured unsteady load distributions.

10. *The Role of Vorticity Convection.*

Previous observations[4] of the transient flow following a sudden change of incidence of a rigid delta wing have shown the important part played by the convection of vorticity in determining the variation of the upper-surface flow with time. Those experiments showed that, following the change of incidence, the flow at a spanwise station at distance x' from the leading apex, reached its steady condition in a time interval that was a close approximation to x'/V, which is the time for the disturbance from the most upstream position, the apex, to be convected to station x'.

For the circumstances of the present experiment, it would be expected from these earlier results that a change in the rate at which vorticity is shed from the leading edge at x will be felt at x' $(>x)$ but only after the convective time delay $\tau=(x'-x)/V$. Furthermore, a change at x that is a harmonic function of ωt will lead to changes of the flow at x', that can be described by a harmonic function of $\omega(t-\tau)$ where $\omega\tau$ represents a phase lag.

To bring the discussion into line with the experimental conclusions regarding the phase lag in the pressure variations, the simplest course seems to be to relate alterations in local incidence to changes in strength of the leading-edge vortices and then to associate these changes in strength with the measured variations in pressure.

A leading-edge vortex of a delta wing can be considered to be fed by the vorticity shed from each point of the leading edge; the strength $\Gamma(x)$ of the vortex at any position x can thus be regarded as being the resultant of the vorticity shed from all positions upstream of x. For an undeformed wing in a steady stream, in accordance with the concept of conical flow, the rate of increase of vortex strength with distance is constant and, at least for small changes, the gradient $d\Gamma/dx$ may be taken to be linear with wing incidence α, so that the increments are related by

$$\Delta\left(\frac{d\Gamma}{dx}\right)=k\Delta\alpha\,. \tag{31}$$

For the wing of the present experiments with static deformation, the strength of each vortex is

$$\Gamma\{x\}=\Gamma_0\{x\}+\bar{\Gamma}\{x\}\,, \tag{32}$$

where Γ_0 represents the contribution due to the mean incidence and $\bar{\Gamma}$ is the perturbation due to deformation. The local incidence varies with chordwise position over the deforming part and can be written

$$\alpha\{x\}=\alpha_0+\bar{\alpha}\{x\}\,, \tag{33}$$

where $\bar{\alpha}$ represents the additional incidence due to deformation. In the subsequent discussion we shall be concerned with only those contributions resulting from the deformation (i.e. $\bar{\Gamma}$ and $\bar{\alpha}$).

As an extension of equation (31), it is assumed that the rate of increase of vortex strength with distance is proportional to *local* incidence, so that

$$\frac{d\bar{\Gamma}}{dx}=k\bar{\alpha}\,. \tag{34}$$

The perturbation in the strength of the vortex at any station downstream of the deformation is then given by the chordwise integral taken over D, the deforming part. That is,

$$\bar{\Gamma}=\int_D \frac{d\bar{\Gamma}}{dx}\,dx=k\int_D \bar{\alpha}\{x\}\,dx\,. \tag{35}$$

Since in this static case the additional incidence $\bar{\alpha}$ is the gradient $(-dz/dx)$,

$$\bar{\Gamma} = kz_0 . \tag{36}$$

The perturbation in strength of the vortex is thus proportional to the deflection at the apex and independent of the shape of the deformation.

In the unsteady case when the deformation is oscillatory, it is assumed that the rate of increase of vortex strength for a point convecting with the flow is proportional to the instantaneous effective incidence

$$\bar{\alpha}_e \equiv -\left(\frac{\partial z}{\partial x} + \frac{1}{V}\frac{\partial z}{\partial t}\right),$$

so that

$$\frac{d\bar{\Gamma}}{dx} = k\bar{\alpha}_e\{x, t\} , \tag{37}$$

the factor k being the same as in equation (34).

The perturbation in the strength of the vortex over the stationary part of the wing now varies both with time and position; for a station at x' at time t', the strength would be the sum of the vorticity shed from each position x at the earlier time $t' - \frac{x'-x}{V}$, and this corresponds to the convective integral of the incidence, that is

$$\bar{\Gamma}\{x', t'\} = k\int_D \bar{\alpha}_e \left\{x, \left(t' - \frac{x'-x}{V}\right)\right\} dx . \tag{38}$$

Because of the form of $\bar{\alpha}_e$, this integral is the difference between the deflection at $x=0$ at time $(t'-x'/V)$ and the deflection at the downstream boundary of the deforming portion, which is always zero, so that

$$\bar{\Gamma}\{x', t'\} = kz\left\{0, \left(t' - \frac{x'}{V}\right)\right\} , \tag{39}$$

or

$$\bar{\Gamma}\{\xi', t'\} = kz_0 \cos(\omega t' - \nu\xi') . \tag{40}$$

In other words, the assumptions that have been made lead to the conclusion that the strength of the vortex has the same phase lag as that found in the measured pressures.

Although the measurements for static deformation show (Section 8.2) that the pressure variations are most easily associated directly with the height and spanwise movements of the vortex above the measuring station, it seems plausible to suggest, that these movements are themselves dependent on the changes in vortex strength. On this basis, the pressures are dependent on the deflection at the apex with an appropriate convective phase delay in the unsteady case. It will be noted that the preceding argument is in accord with the experimental conclusions relating both to the equality of pressure amplitude for a quasi-steady variation and an oscillatory condition and to the magnitude of the phase lag.

11. *Comparison with Slender-Wing Theories.*

An essential feature of slender-wing theory is the attention given to the flow components in transverse or cross-flow planes. In the present discussion, rather than considering the flow at a particular chordwise position of the wing, we find it convenient to consider the behaviour of the fluid as it passes the wing. Then on the assumption of the theory, the fluid can be regarded as remaining in plane transverse slabs as it moves downstream; the unsteady flow in these planes is treated as two-dimensional and the reactions

on the wing are determined by the cross flow. Each travelling cross-flow plane 'sees' a certain wing distortion so that, considered in this way, the theory is as applicable to unsteady as to steady motion. For a wing in steady motion all cross-flow planes see the same deformation; for a wing in unsteady motion, in general, each plane sees a different deformation.

As sketched in Fig. 41(a) basic slender-wing theory assumes irrotational flow in transverse planes. and the local reaction on the wing is related solely to the time rate of change of downward momentum in the travelling plane. That is, the flow and loading at any section are dependent only on the local rates of change of effective incidence and span occurring at that section; because of the irrotational assumption and thus an absence of shed vorticity, the flow field in a transverse plane contains no history of its passage over the upstream part of the wing. Wing loading at a transverse section of the wing is independent of changes occurring elsewhere. For the present experiment this theory is clearly unsatisfactory because it predicts no changes in pressure downstream of the deforming part of the wing.

Extensions to the original slender-wing theory that take account of leading-edge separation have already been discussed in papers by Hancock[5], Lowson[6], Randall[7] and Dore[8]; in the present discussion we are concerned only with general considerations and not with the particular mathematical models of leading-edge separation used by these authors. As before, we consider transverse planes moving with stream velocity, but now, because the flow separates from the side edges, vorticity is shed into the cross-flow planes and this leads to the formation of the two vortices sketched in Fig. 41(b). Thus, unlike the irrotational model, the cross-flow planes contain a record of their previous history by virtue of the shed vorticity which is convected with them. Thus the flow and wing loading at chordwise position x' and time t' can now be associated not only with the local instantaneous conditions at (x', t') but also with the conditions previously experienced by that particular fluid plane now at x'. That is, the unsteady pressure distribution at (x', t') can be related to an equivalent steady deformation of the wing, namely the deformation previously experienced by the travelling plane designated (x', t').

In the present case the unsteady deformation is defined by

$$z = \bar{z}_0 F(\xi) \cos \omega t \,. \tag{41}$$

When the cross-flow plane (x', t') was previously at $x\,(<x')$, the deflection which the wing then had may be obtained from equation (41) by putting $t = [t' - (x' - x)V]$. Thus the apparent mode of wing deformation experienced by plane $(x't')$ as it moves across the wing is

$$z = \bar{z}_0 F(\xi) \cos \omega \left[t' - (x' - x)/V\right] = \bar{z}_0 F(\xi) \cos \left[\omega t' - \nu(\xi' - \xi)\right] . \tag{42}$$

This is the equivalent steady deformation, and we note that each combination of (ξ', t') within a cycle requires a different equivalent mode*.

Now the experiment has shown that an instantaneous pressure at (ξ', t') matches that for the steady deformation

$$z = \bar{z}_0 F(\xi) \cos (\omega t' - \nu\xi') \,. \tag{43}$$

However, this mode of deformation is not the same as that given by equation (42) except for the deflections at the apex. This difference is to some extent explained by the argument of the previous section, which deduced that the shape of the deformation did not affect the pressure. However, without the assumptions necessary for that argument, we note that it is unlikely that a unique relationship exists between spanwise pressure distribution and the mode of deformation. It seems that a given spanwise pressure distribution could be produced by a set of static deformation modes; thus the experimental results do not necessarily

* It would have been useful to have deformed the wing statically to conform to a series of modes given by equation (42) and to have measured the pressure distributions for these. Unfortunately, the experimental programme was completed before the value of such measurements was realised.

negate the equivalent static mode deduced theoretically. We may, however, expect that for each member of such a set of modes the weighted mean of some characteristic quantity taken over the deforming part would be the same. Now the integrals of the chordwise distribution of incidence are identical for the modes of equations (42) and (43). Hence, if the relationship in Section 10 between pressure change and the integral of the change of local incidence is accepted, the results of the experiment lend support to the extension of slender-wing theory that takes account of the vortices.

It is necessary to put the matter in a broader perspective. Disturbances in a moving fluid are propagated either acoustically or by streamwise convection. If we consider the basic case of a disturbance point at x and an observation point at x', then, although in subsonic flow disturbances will propagate acoustically from x to x' whatever the relative disposition of the two points, propagation by convection will only occur if x is upstream of x'. Now the limitations of the present experimental conditions preclude any examination of the pressure changes occurring when the observation point, i.e., the pressure measuring station, is itself undergoing unsteady motion or when it is upstream of the disturbance (i.e., the deforming portion of the wing). The experimental results refer only to the condition in which the disturbance is upstream of the observation point; within this restriction the results show convection to be dominant and seem to validate a convective slender-wing-approach. But it must be realised that such a theory denies pressure changes due to disturbances downstream of the observation point.

12. *Concluding Remarks.*

12.1. *Summary of experimental results.*

(1) Pressure variations over regions of the upper surface of the wing directly influenced by the vortex flow exhibit pronounced non-linearities; for sinusoidal motion they contain appreciable higher harmonic components.

(2) Pressure variations at different points of a transverse plane are approximately in phase, or anti-phase, with one another. That is, the phase difference between the loading and the deformation is constant across the span (ε independent of η).

(3) The amplitudes of the Fourier components of the pressure variation appear to be independent of frequency. For any given chordwise position, the pressure variations during an oscillation are approximately the same as those for a corresponding quasi-steady variation ($R(\eta) \simeq |S(\eta)|$), except that there is a phase delay between the pressures and the deformation.

(4) For a given frequency, the phase delay appears to be linearly related to chordwise distance from the leading apex.

(5) For a given chordwise position, the phase delay is proportional to frequency.

(6) The time lag associated with the phase delay is approximately equal to the time taken for convection from the apex of the wing to the particular chordwise position.

(7) Collectively, the above conclusions (2) to (6) lead to a relationship between the unsteady spanwise pressure distributions and those measured for steady conditions. This relationship is expressed in terms of frequency parameter ν and chordwise co-ordinate, ξ by the formula,

$$\Delta C_p(\eta) = S_0(\eta) + S_1(\eta) \cos(\omega t - \nu\xi) + S_2 \cos 2(\omega t - \nu\xi) + \ldots,$$

where $S(\eta)$ is the distribution of a harmonic component for a quasi-steady variation and is dependent only on amplitude of deformation and ξ. Alternatively, the results indicate that the oscillatory loading at position ξ' and time t' matches the loading at ξ' for a steady deformation

$$z = \bar{z}_0 F(\xi) \cos(\omega t' - \nu\xi').$$

12.2. *General implications.*

Any conclusions concerning the pressure distribution over a highly swept deforming wing that are drawn from the present experiments must be conditional, because the deformation was entirely upstream of the measuring stations. Further experiments which would complement the present ones would examine

the pressure variation due to local deformation downstream of the measuring station. A more comprehensive investigation would require measurements of the complete pressure distribution on a wing, the whole of which is undergoing deformation; that is, measurements of the type described in Ref. 1 but with a wing set at sufficient incidence for vortex flow to occur.

However, even in the absence of wider experimental evidence, certain general considerations regarding the effects of vortex flow follow from the present experimental results. For motions or deformations that lead to alterations in the positions of the vortices, non-linearities are likely to be present in the relationship between local pressure and displacement. Indeed, it can be stated that any situation in which the position of the vortex moves relative to the wing, whether this be caused by motion or deformation of the wing or by turbulence inherent in the oncoming stream, is likely to lead to large-amplitude pressure fluctuations in the neighbourhood of the peak suction. If the vortex movements are periodic with frequency ω, the pressure fluctuations in the region of the wing directly under the influence of the vortex will contain harmonic components with frequencies ω, 2ω, 3ω etc. If a flexible structure is subjected to such pressure variations, then it is possible for responses to be excited at the higher harmonics as well as the fundamental frequency. In principal, then, we have a mechanism whereby a sinusoidal excitation at one frequency can lead to structural responses at multiples of this frequency. In practice, the importance of this phenomenon would depend on the degree to which the spatial distribution of the pressure variations matches the shape of the normal modes of wing distortion that have natural frequencies close to multiples of the fundamental excitation frequency.

It is relevant to remark that the kind of non-linear effects discussed above are not peculiar to wings with leading-edge separation. Analogous examples could be found in oscillatory motions involving either the chordwise movement of the suction peak at the leading edge of a wing with attached flow or the movements of a shock wave over the surface of a wing. The common factor leading to such effects is the presence of steep gradients in the spatial distribution of surface pressure and an imposed variation in the positions of these gradients.

It has already been shown in Ref. 1 that for a slender delta wing at zero incidence, and therefore with flow attached at the leading edges, lifting-surface calculations give unsteady pressure distributions in reasonable agreement with measurements. The present experiments draw attention to the need for a similar method to deal with unsteady pressure distributions for wings with vortex flow.

LIST OF SYMBOLS

A_n, B_n	Fourier coefficients relating to cyclic variation of pressure, equation (9)
a_1, b_1	Normalized versions of A_1, B_1, equations (13) and (14)
C_p	Non-dimensional pressure coefficient, equation (6)
ΔC_p	Non-dimensional pressure difference between upper and lower surfaces of wing, equation (7)
c_0	Centre-line chord of wing
$C_L(\xi)$	$\int_0^1 \Delta C_p(\xi, \eta) d\eta$, spanwise sectional lift coefficient
$F(\xi)$	Mode of wing deformation, equation (1)
$F'(\xi)$	$dF/d\xi$
H	Measure of higher harmonic content of pressure variation, equations (11) and (12)
k_1, k_2, k	Constants in equations (17), (18) and (31) respectively
L_n	Fourier coefficients relating to cyclic variation of spanwise sectional lift, equation (30)
n	Integer defining order of harmonic component
p	Pressure
R_n	$(A_n^2 + B_n^2)^{\frac{1}{2}}$, Fourier coefficient relating to cyclic variation of pressure; equation (8)
Re	Reynolds number based on centre-line chord, c_0
S_n	Fourier coefficient relating to quasi-steady variation of pressure, equation (10)
s	Local semi-span
s_0	Trailing-edge semi-span
t	Time
V	Stream velocity
x, y	Geometrical co-ordinates, Fig. 1
z	Upward deflection of a point on deforming portion of wing
z_0	Value of z at leading apex
$\bar{z}_0$	Amplitude of oscillatory displacement at apex
α	Incidence
α_0	Incidence of rigid part of wing; mean incidence of deforming part
$\bar{\alpha}$	Additional incidence due to deformation, equation (33)
Γ	Strength of vortex, equation (32)
Γ_0	Value of Γ when wing undeformed, equation (32)
$\bar{\Gamma}$	Increment in Γ due to deformation, equation (32)
ε_n	Phase delay associated with n^{th} harmonic component, equation (8)

ε'_n	ε_n or $\varepsilon_n - \pi$
ζ_0	z_0/c_0, non-dimensional displacement at leading apex
$\bar{\zeta}_0$	Amplitude of ζ_0
η	y/s, non-dimensional co-ordinate
ξ	x/c_0, non-dimensional co-ordinate
μ	Viscosity
ν	$\omega c_0/V$, frequency parameter
ρ	Air density
τ	Time delay
ϕ	Angular co-ordinate describing oscillation, equation (2)
ω	Angular frequency of oscillation rad/s

REFERENCES

No.	*Author(s)*	*Title, etc.*
1	F. Ruddlesden, D. A. Drane and P. W. Slaven	Oscillatory pressure measurements on a flexible slender wing model at low subsonic speeds. A.R.C. R. & M. 3596 (1967).
2	D. W. Bryer, M. J. Larcombe and J. F. M. Maybrey	Note on the use of certain pressure transducers for surface pressure plotting on a wing undergoing oscillatory deformation in a low-speed wind tunnel. N.P.L. Aero. Memo 22. 1965.
3	R. F. A. Keating	Measurement of pressures on a delta wing oscillating in heave at a high angle of incidence. R.A.E. Report 67241. 1967. A.R.C. 29 895.
4	N. C. Lambourne, D. W. Bryer and J. F. M. Maybrey	The behaviour of the leading-edge vortices over a delta wing following a sudden change of incidence. A.R.C. R. & M. 3645 (1969).
5	G. J. Hancock	On the transient motion of a slender delta wing with leading-edge separation. A.R.C. C.P. 563. (1960).
6	M. V. Lowson	The separated flows on slender wings in unsteady motion. A.R.C. R. & M. 3448. (1963).
7	D. G. Randall	Oscillating slender wings with leading-edge separation. Aero. Quart. Vol. XVII. Part 4. November 1966.
8	B. D. Dore	The unsteady motion of slender wings with leading edge vortices. A.R.C. C.P. 810. (1964).
9	H. C. Garner and D. A. Fox	Algol 60 Programme for Multhopp's low-frequency subsonic lifting-surface theory. A.R.C. R. & M. 3517. (1966).

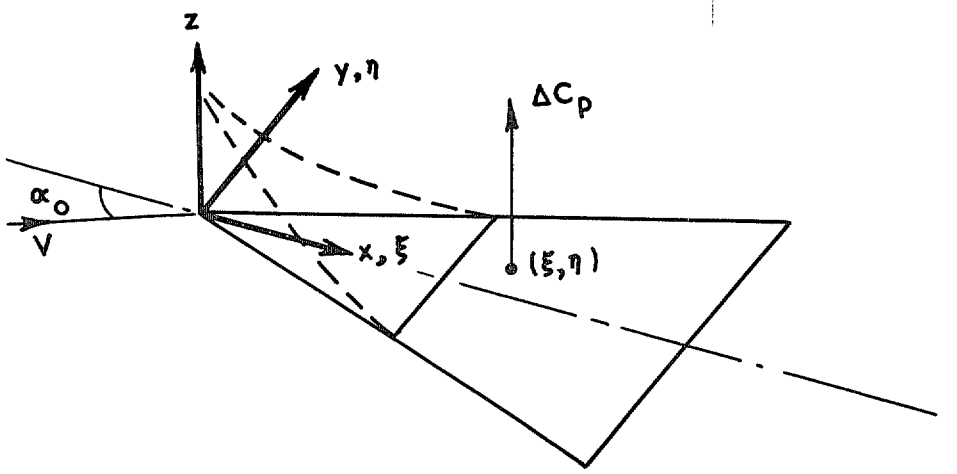

FIG. 1. Coordinate system.

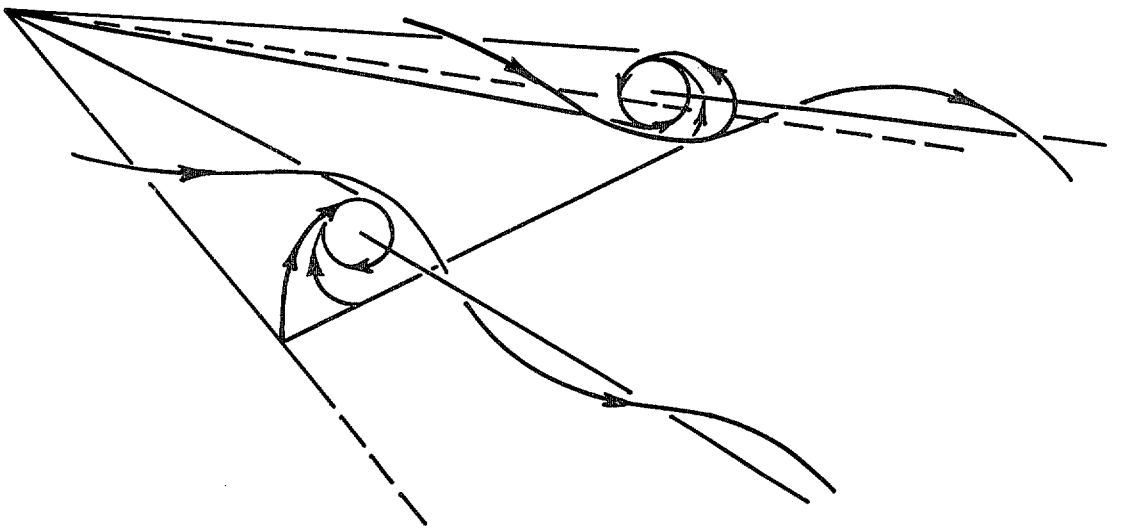

FIG. 2. Vortex flow over upper surface of undeformed delta wing.

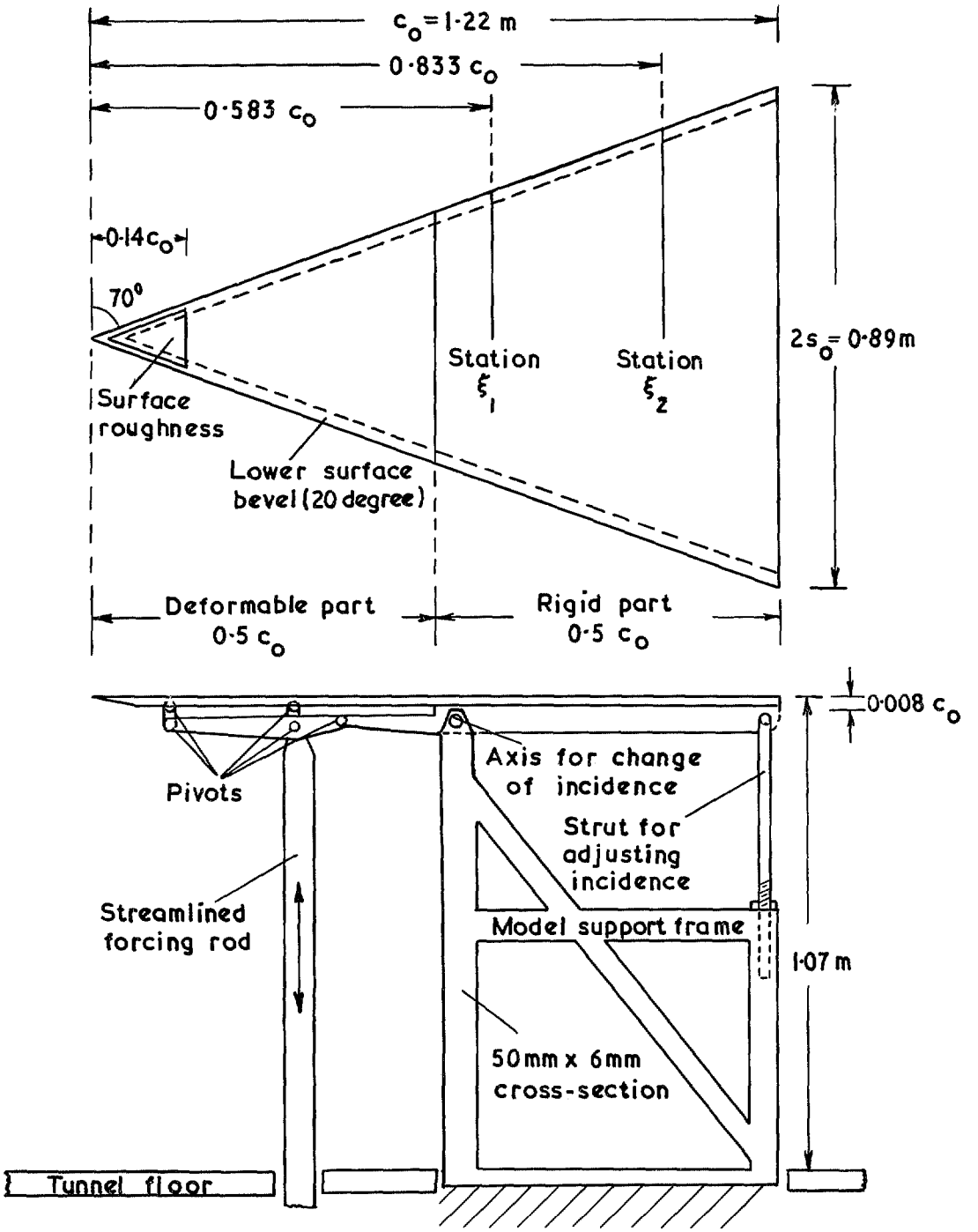

FIG. 3. General dimensions of model and support system in 9ft × 7ft (2·7m × 2·1m) tunnel.

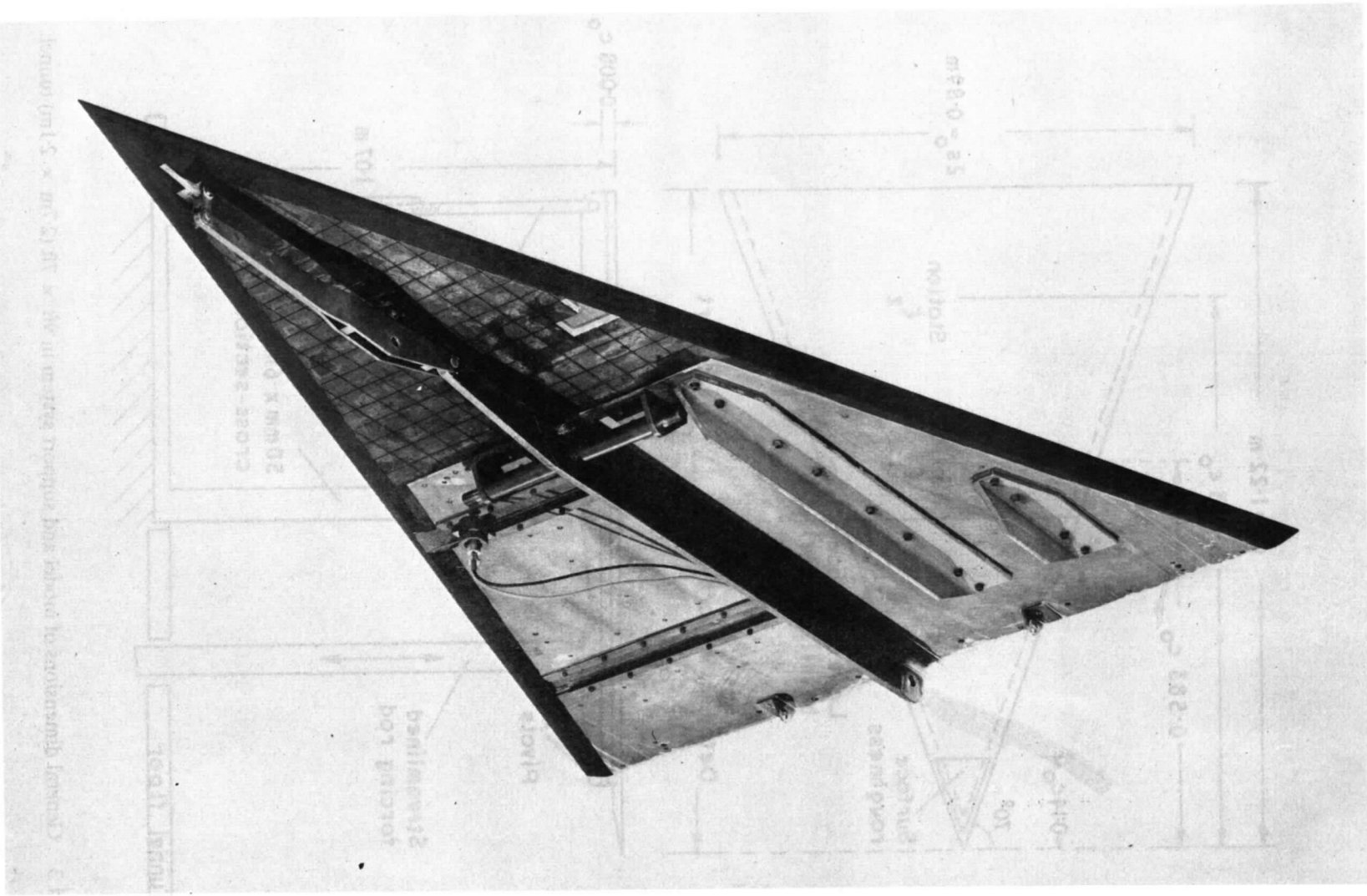

FIG. 4. View of underside of model.

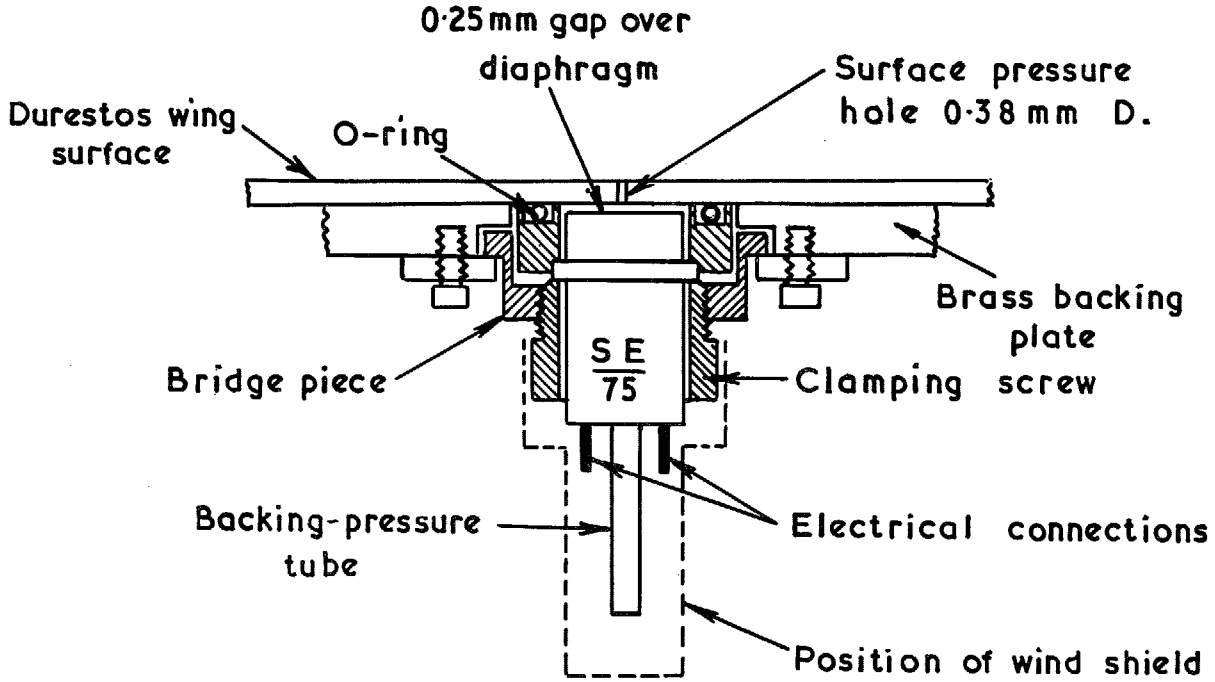

FIG. 5. Pressure transducer mounting.

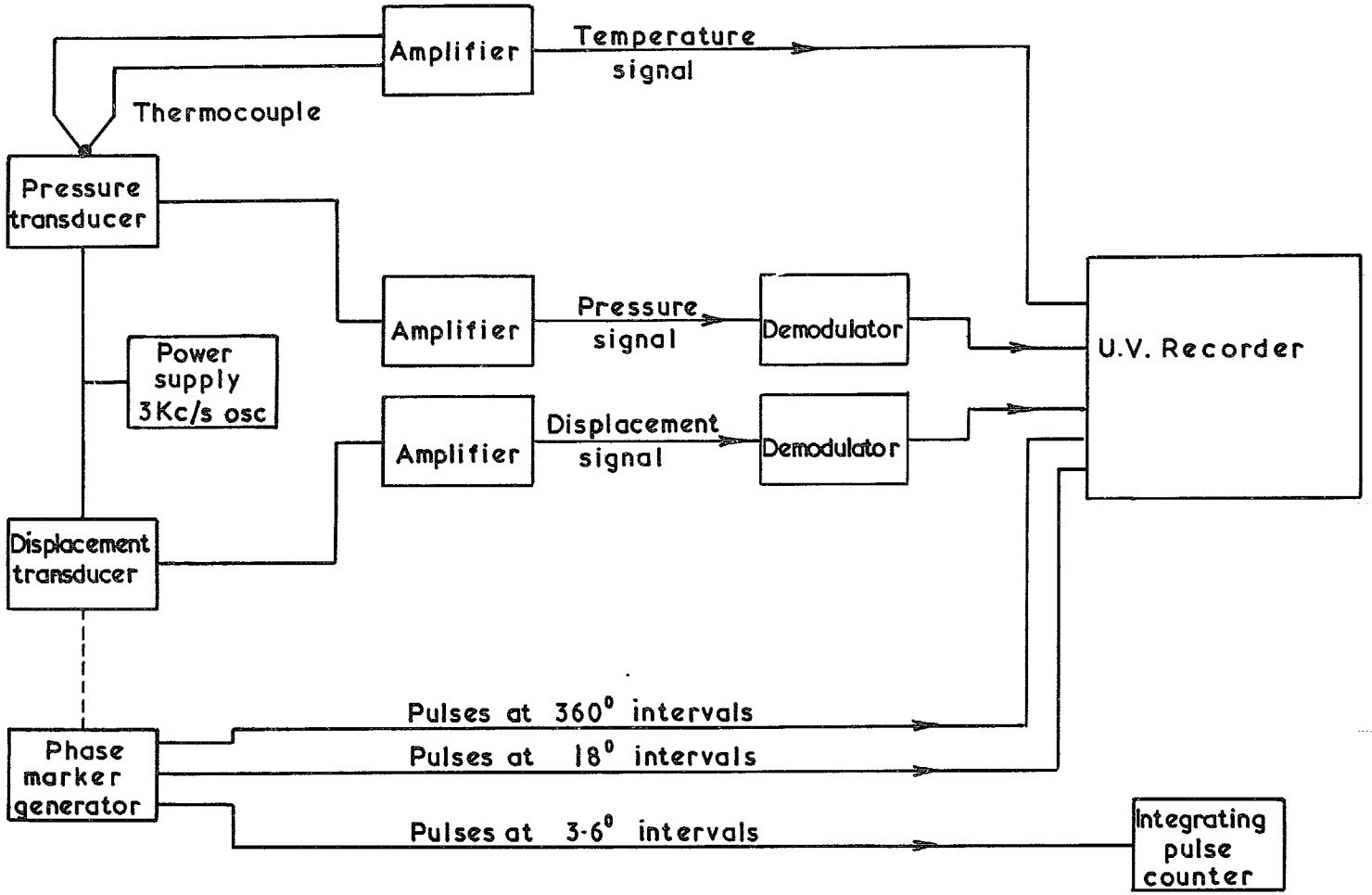

FIG. 6. Block diagram of instrumentation.

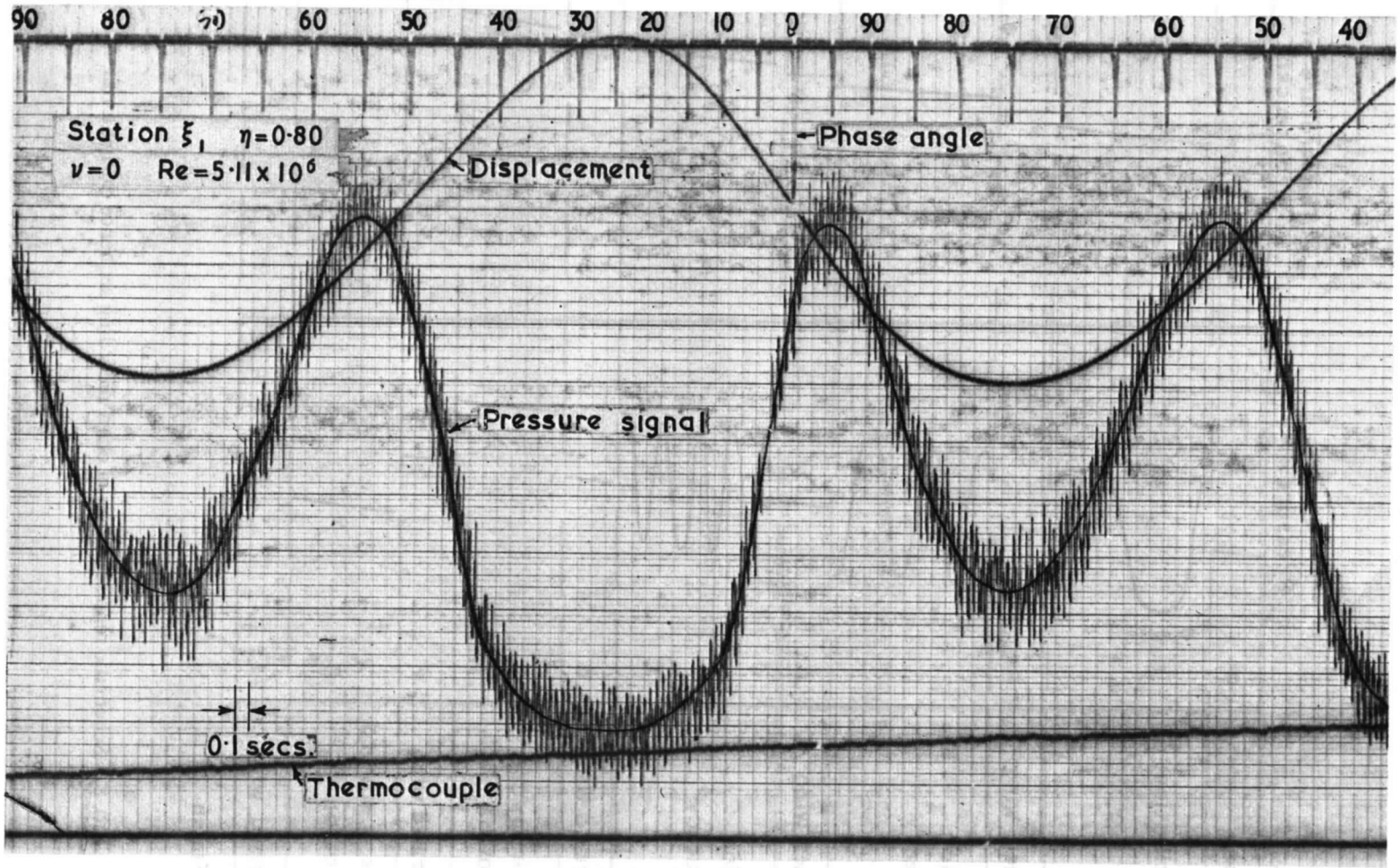

FIG. 7. Example of chart record.

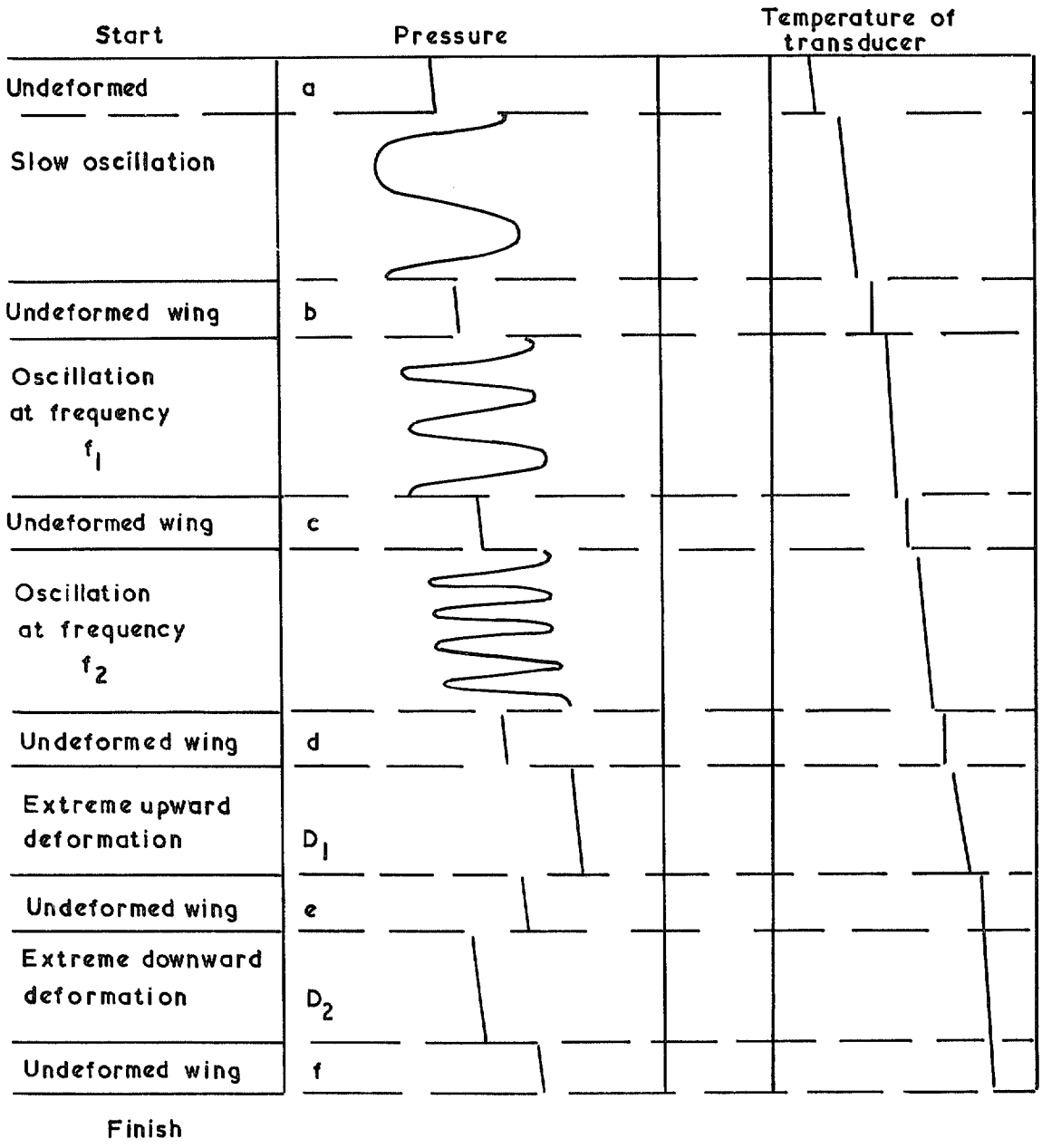

FIG. 8. Schematic representation of chart recording sequence during a run.

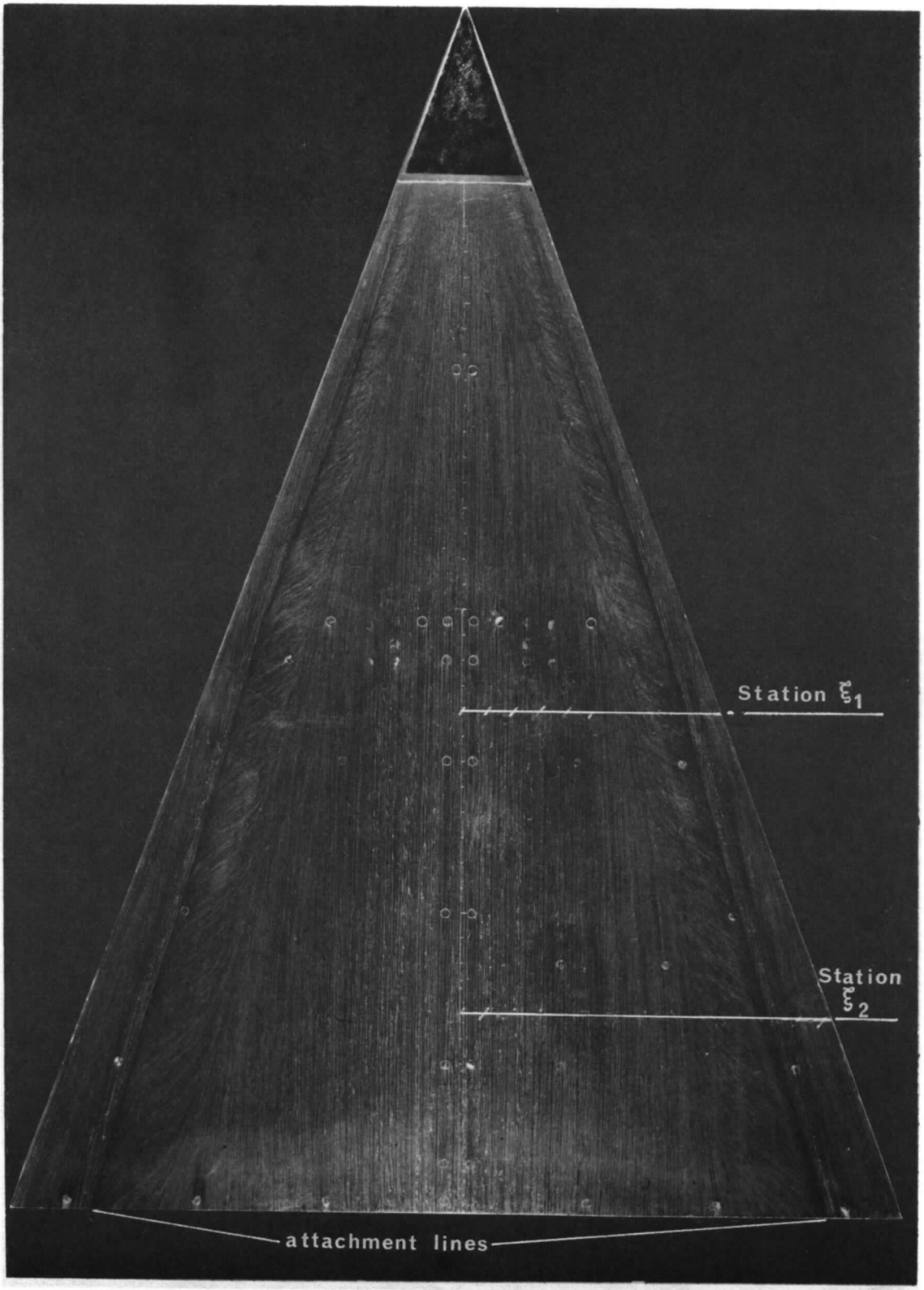

FIG. 9. Oil flow pattern undeformed wing ($\zeta_0 = 0$)
Nominal incidence 5 degrees, $Re = 2{\cdot}6.\ 10^6$.

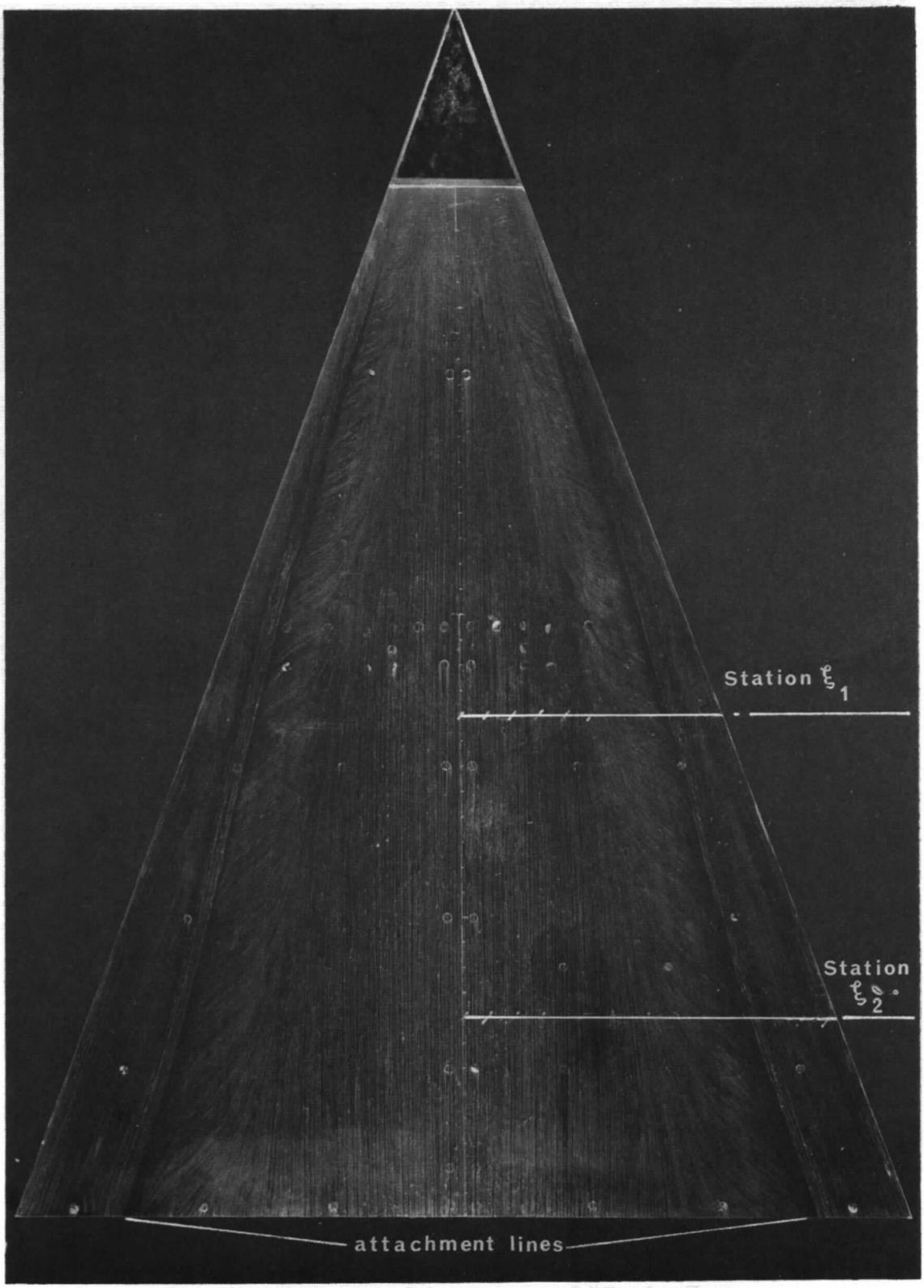

FIG. 10. Oil flow pattern wing bent up ($\zeta_0 = 0{\cdot}0262$).
Nominal incidence 5 degrees, $Re = 2{\cdot}6.\ 10^6$.

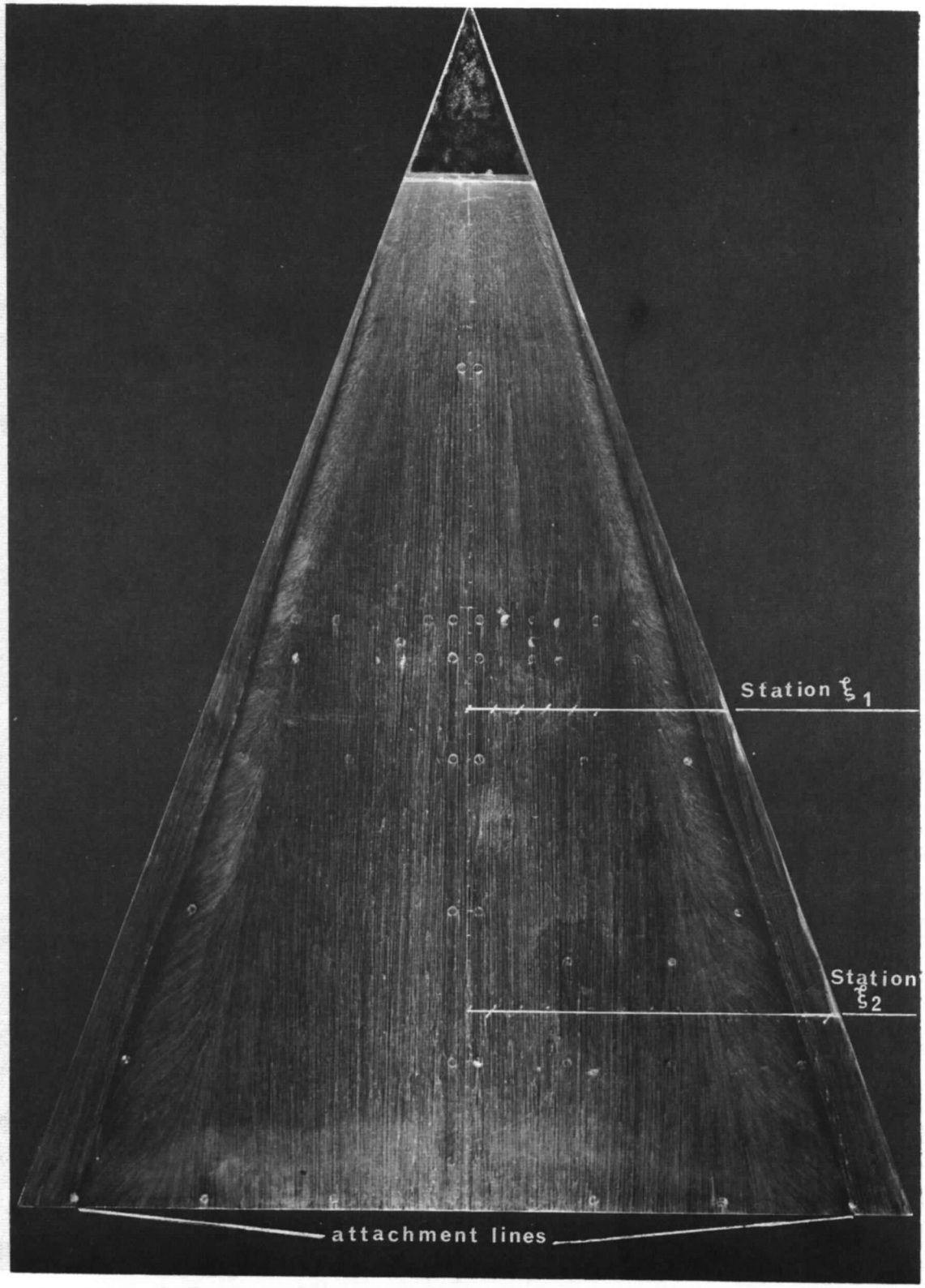

FIG. 11. Oil flow pattern wing bent down ($\zeta_0 = -0{\cdot}0262$). Nominal incidence 5 degrees, $Re = 2{\cdot}56.\ 10^6$.

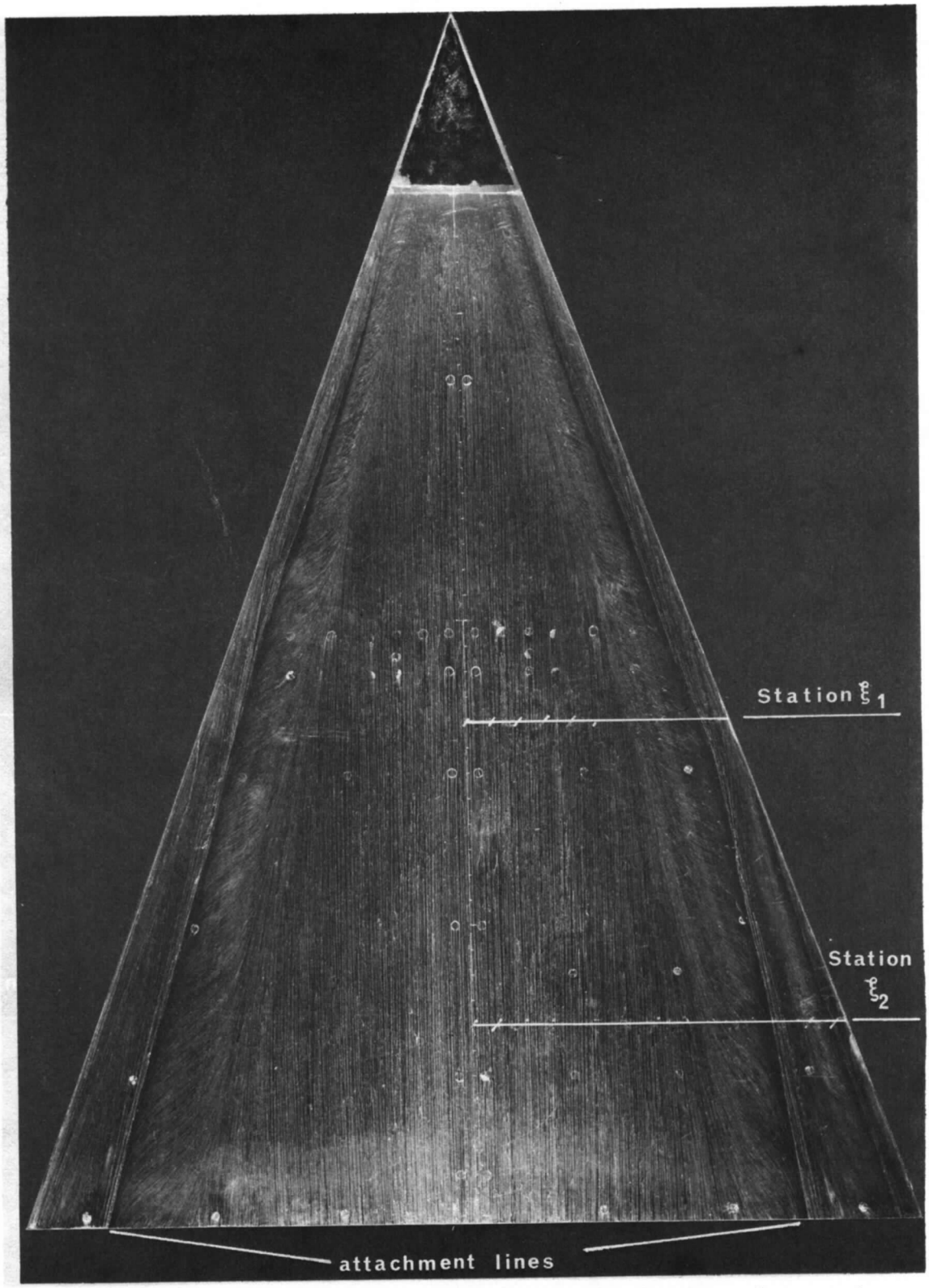

FIG. 12. Oil flow pattern undeformed wing ($\zeta_0 = 0$). Showing flow interference from transducer at station ξ_1, $\eta = 0{\cdot}9$. Nominal incidence 5 degrees, $Re = 2{\cdot}6.\ 10^6$.

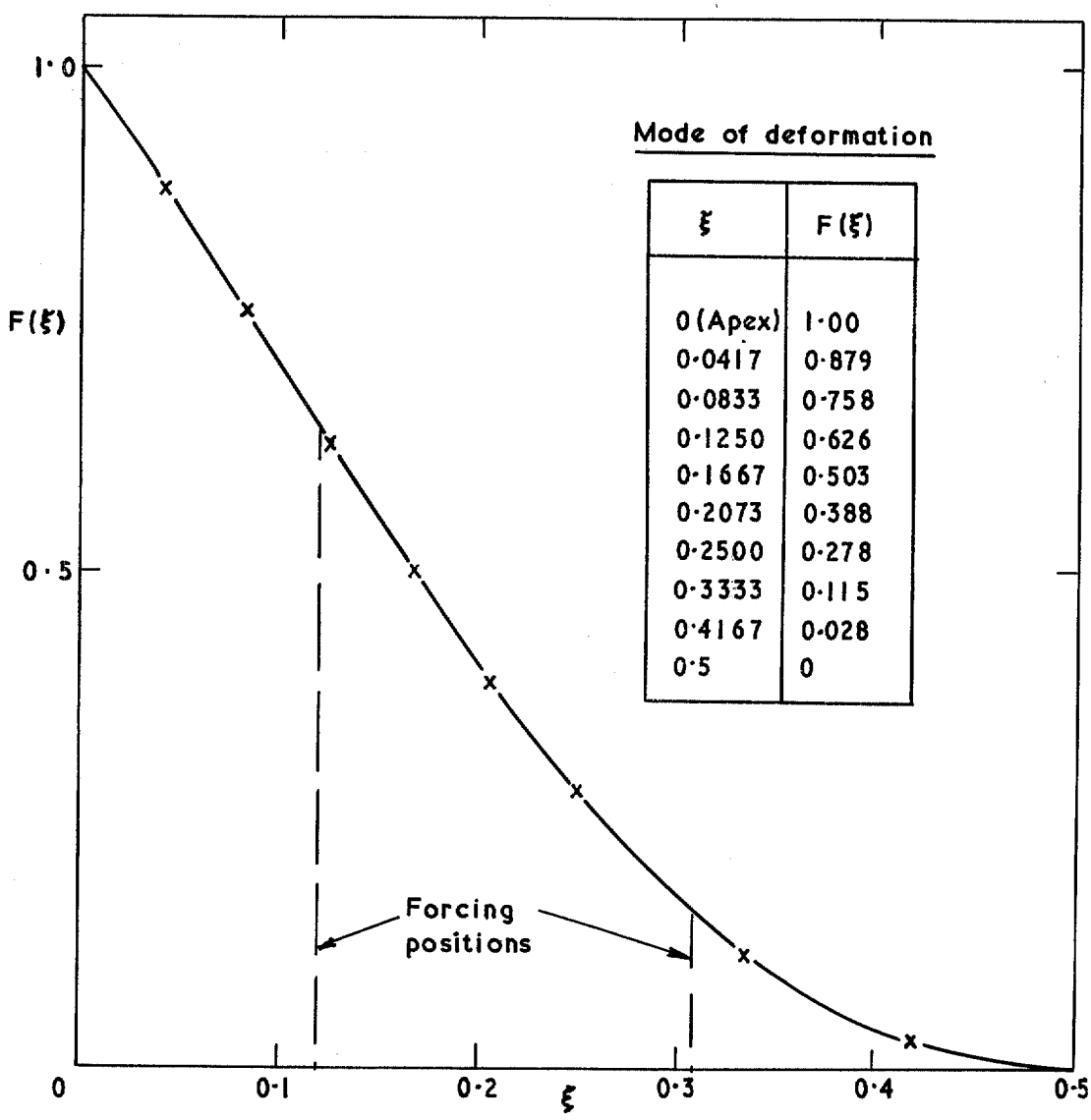

FIG. 13. Mode of deformation.

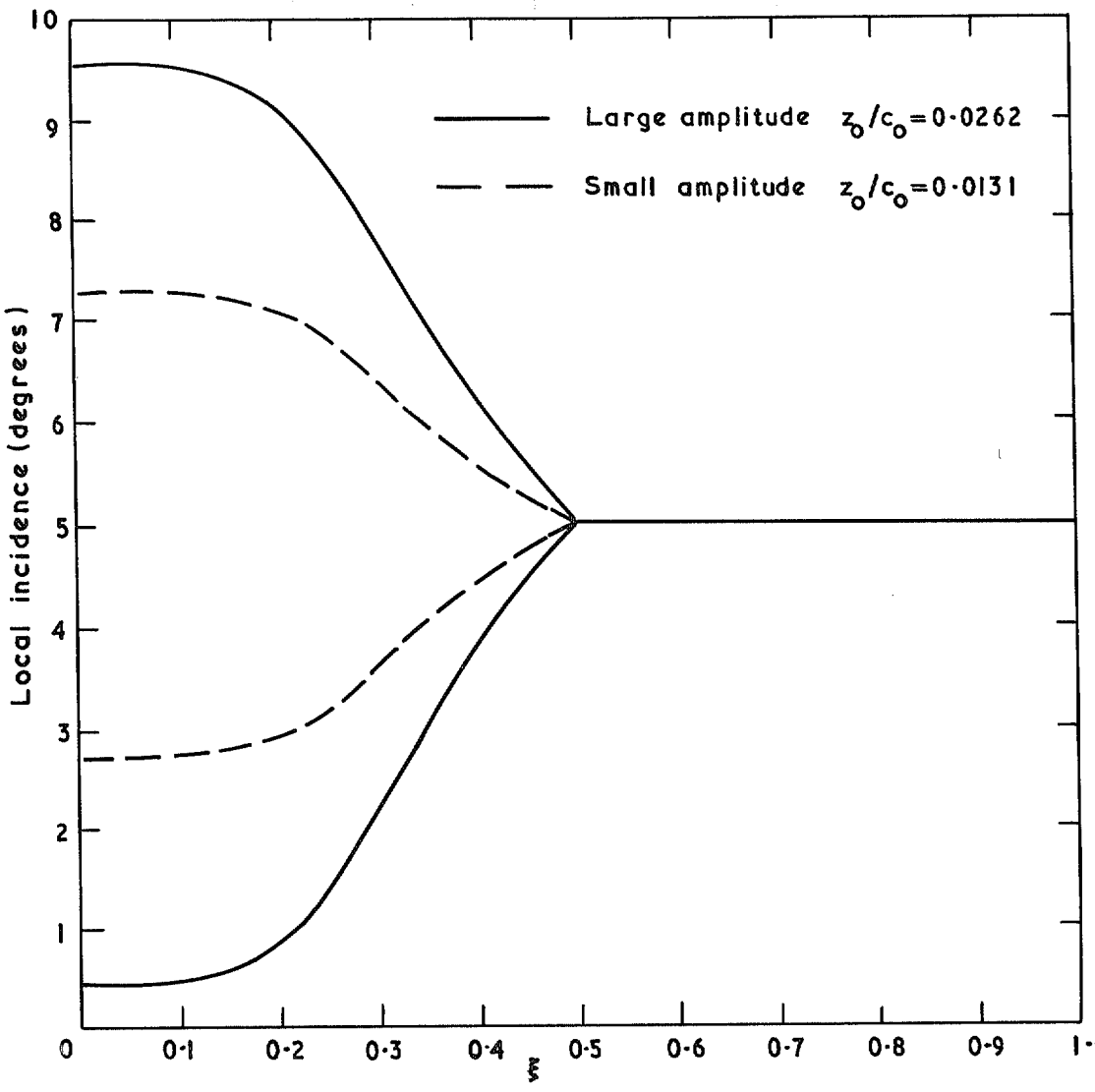

FIG. 14. Chordwise variation of local incidence due to steady deformation.

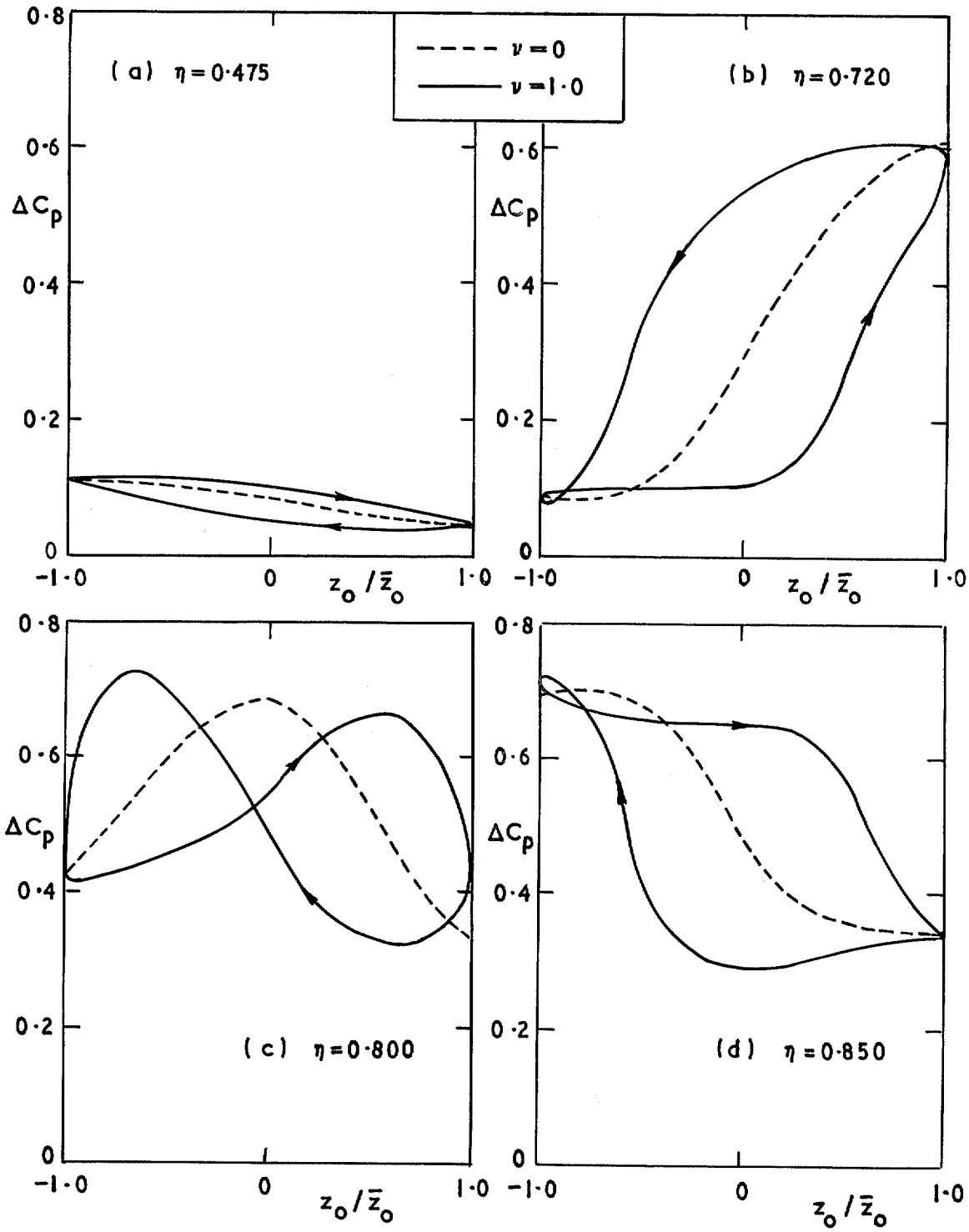

FIG. 15. Variation of ΔC_p with cyclic wing deformation for different spanwise positions. ξ_1 ($\equiv 0{\cdot}583$), $\bar{z}_0/c_0 = 0{\cdot}0262$, $Re = 2{\cdot}56 \times 10^6$.

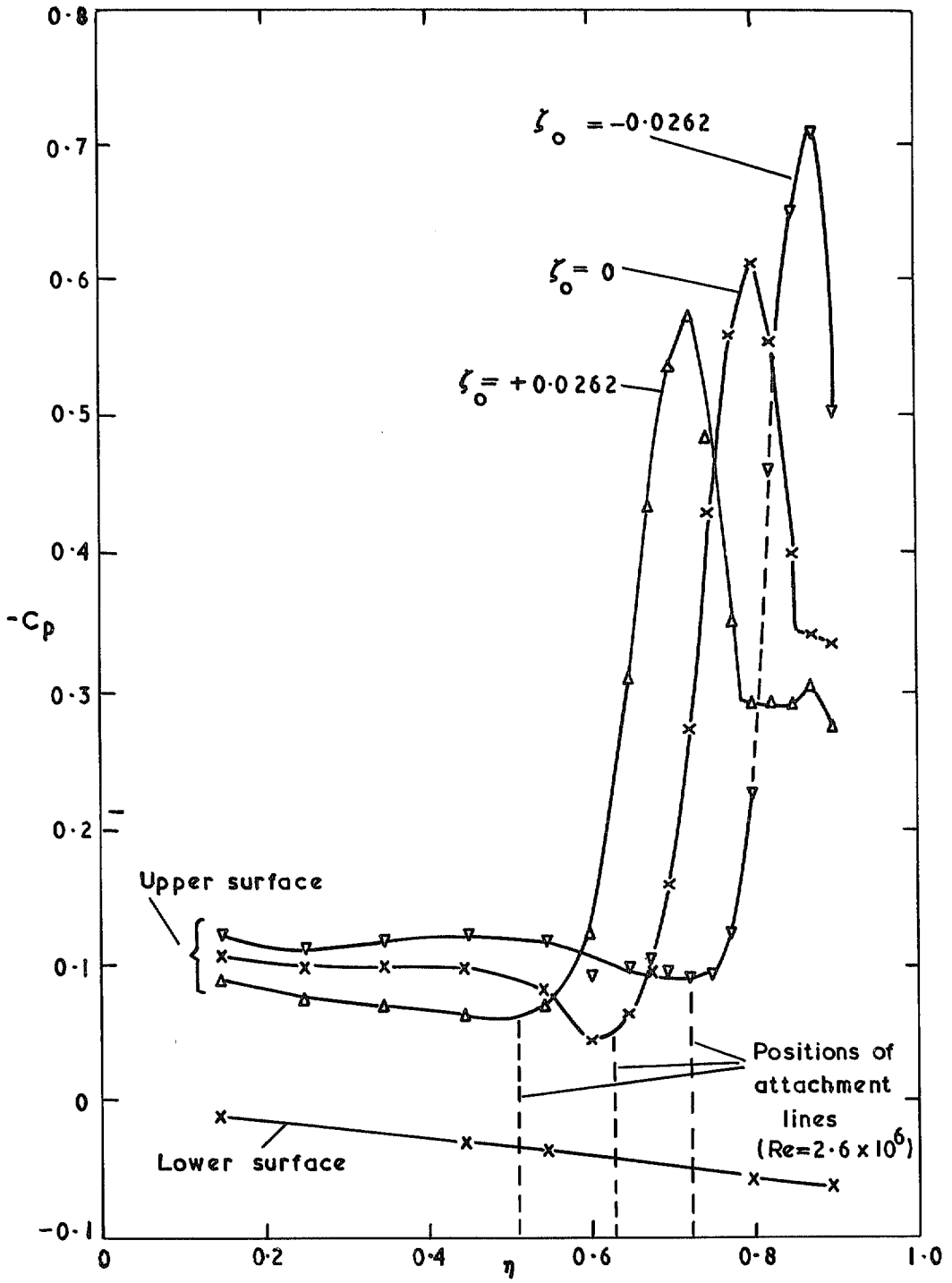

FIG. 16. Spanwise pressure distribution for steady deformation. Station ξ_1, $Re = 5{\cdot}11 \times 10^6$.

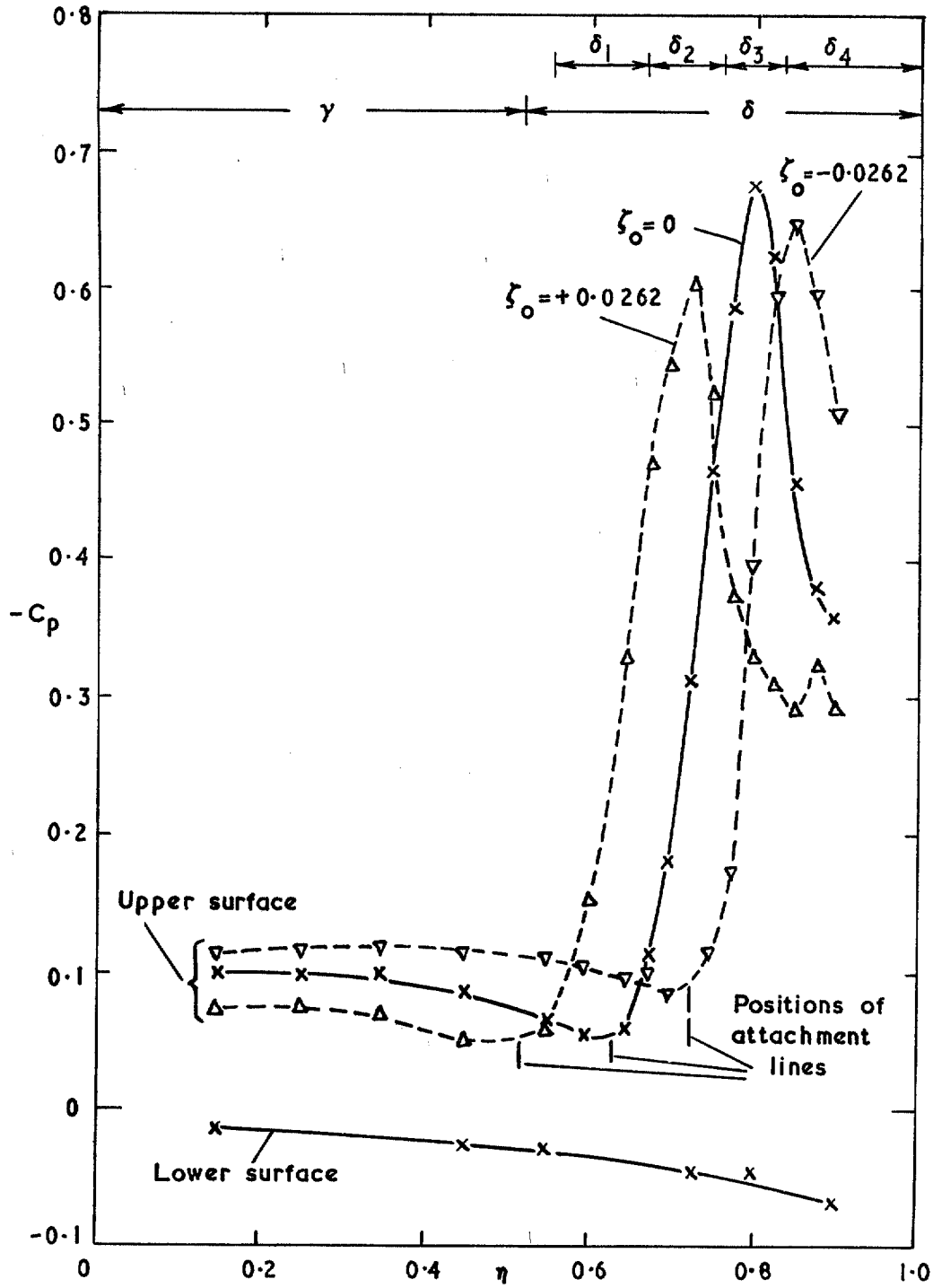

FIG. 17. Spanwise pressure distribution for steady deformations. Station ξ_1, $Re = 2{\cdot}56 \times 10^6$.

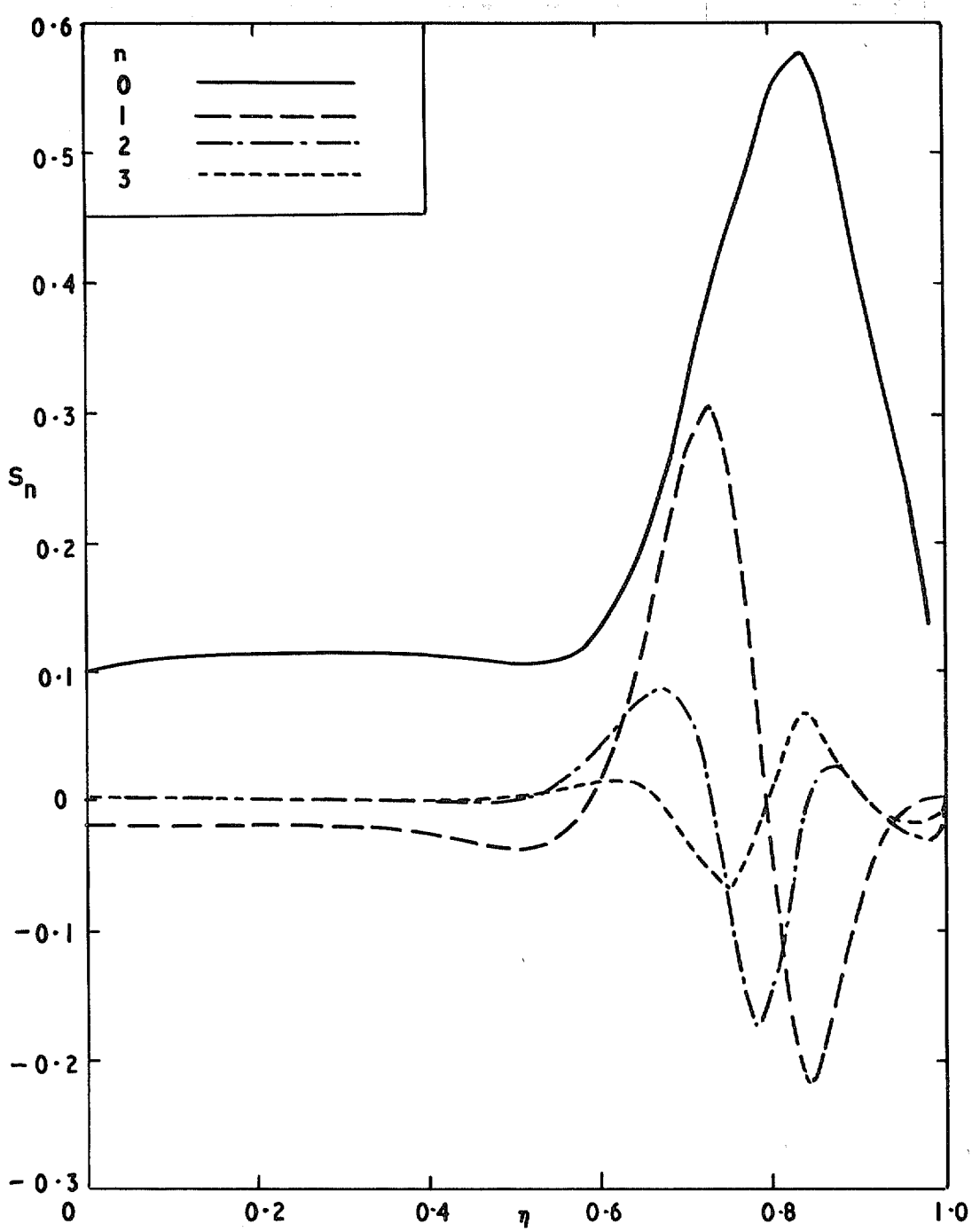

FIG. 18. Spanwise distributions of harmonic components (S_n) for quasi-steady variation. Station ξ_1, $\bar{\zeta}_0 = 0{\cdot}0262$, $v = 0$, $Re = 2{\cdot}56 \times 10^6$.

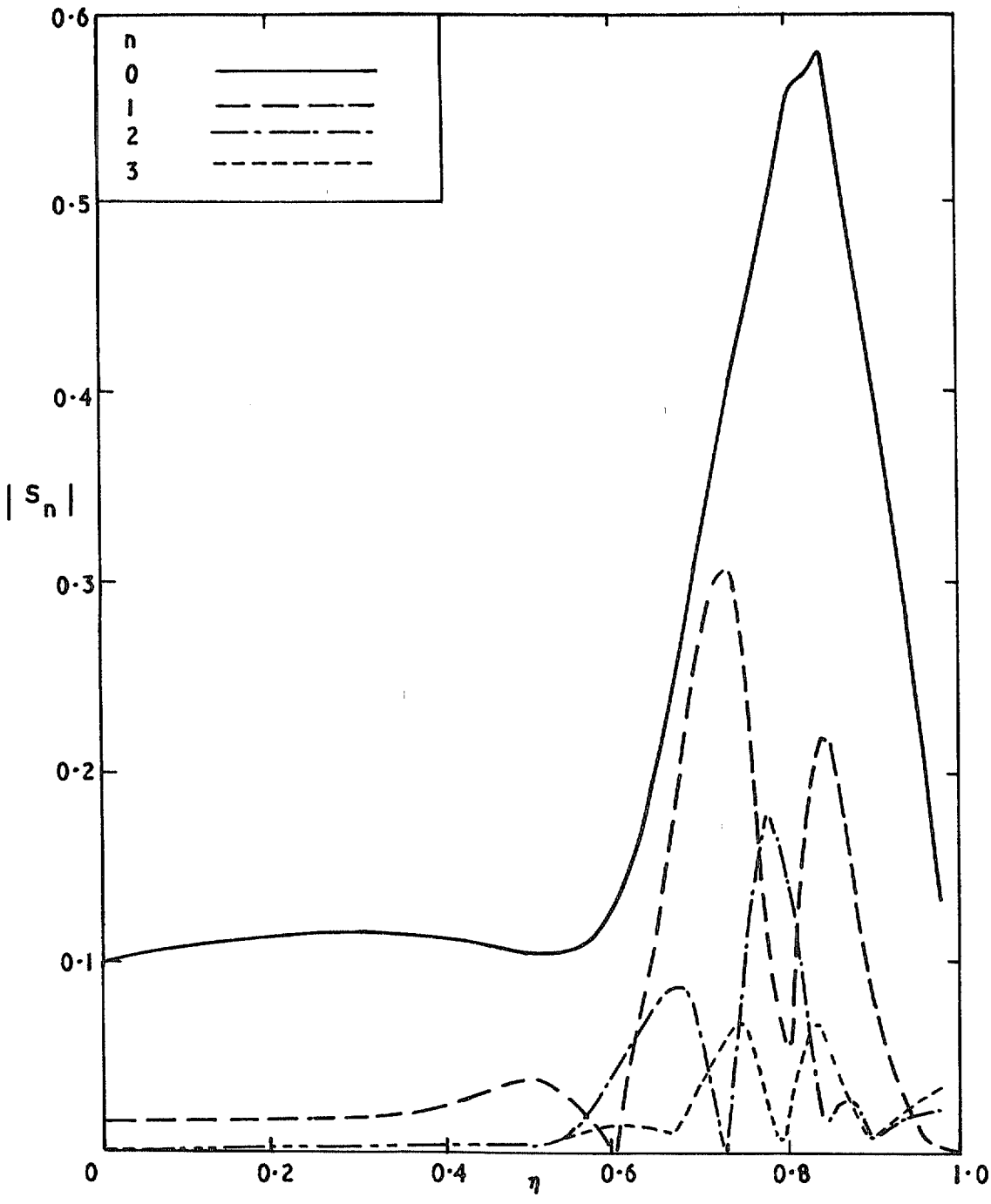

FIG. 19. Spanwise distributions of harmonic components ($|S_n|$) for quasi-steady variation. Station ξ_1, $\bar{\zeta}_0 = 0{\cdot}0262$, $v = 0$, $Re = 2{\cdot}56 \times 10^6$.

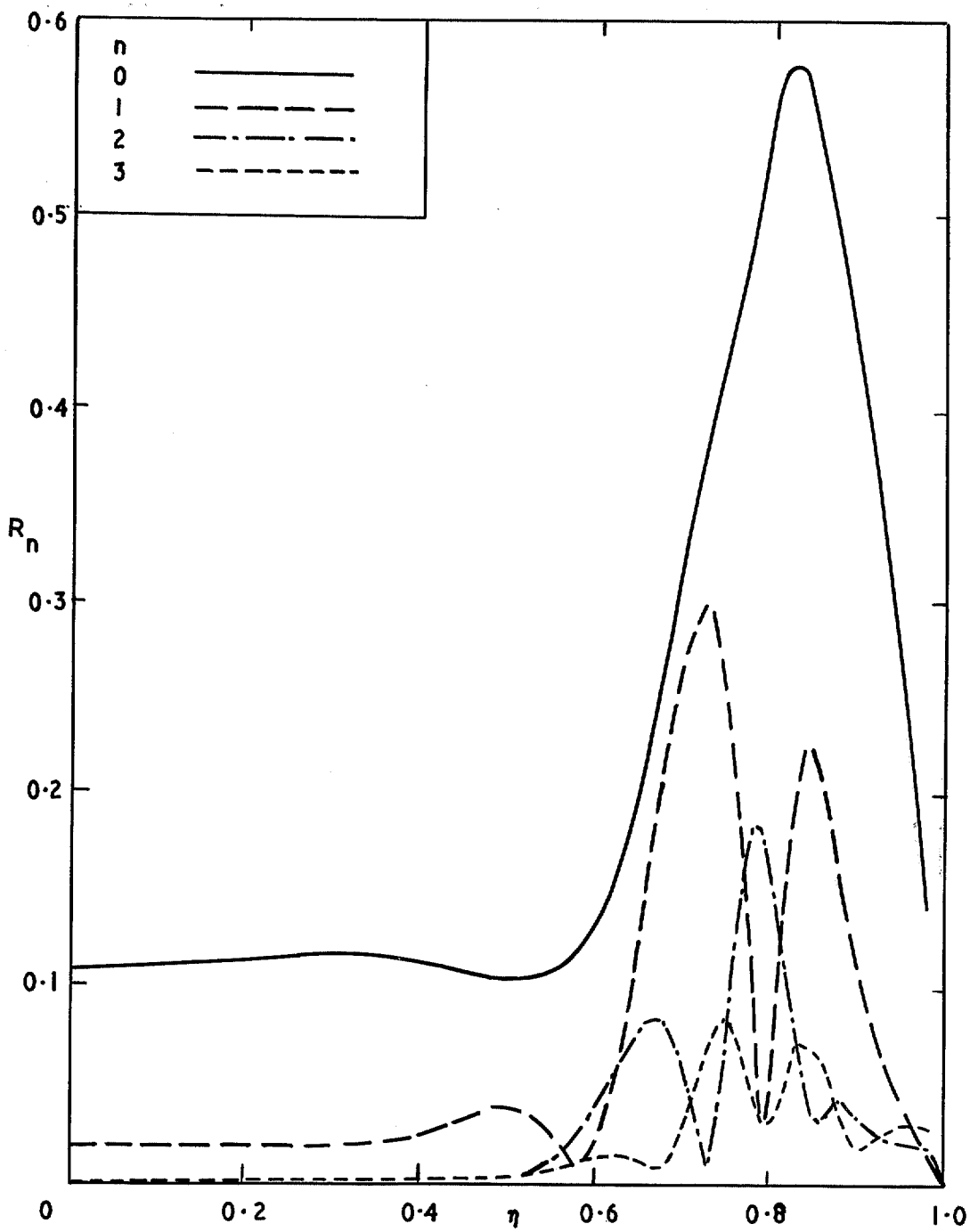

FIG. 20. Spanwise distributions of harmonic components (R_n).
Station ξ_1, $\bar{\zeta}_0 = 0{\cdot}0262$, $v = 1{\cdot}0$, $Re = 2{\cdot}56 \times 10^6$.

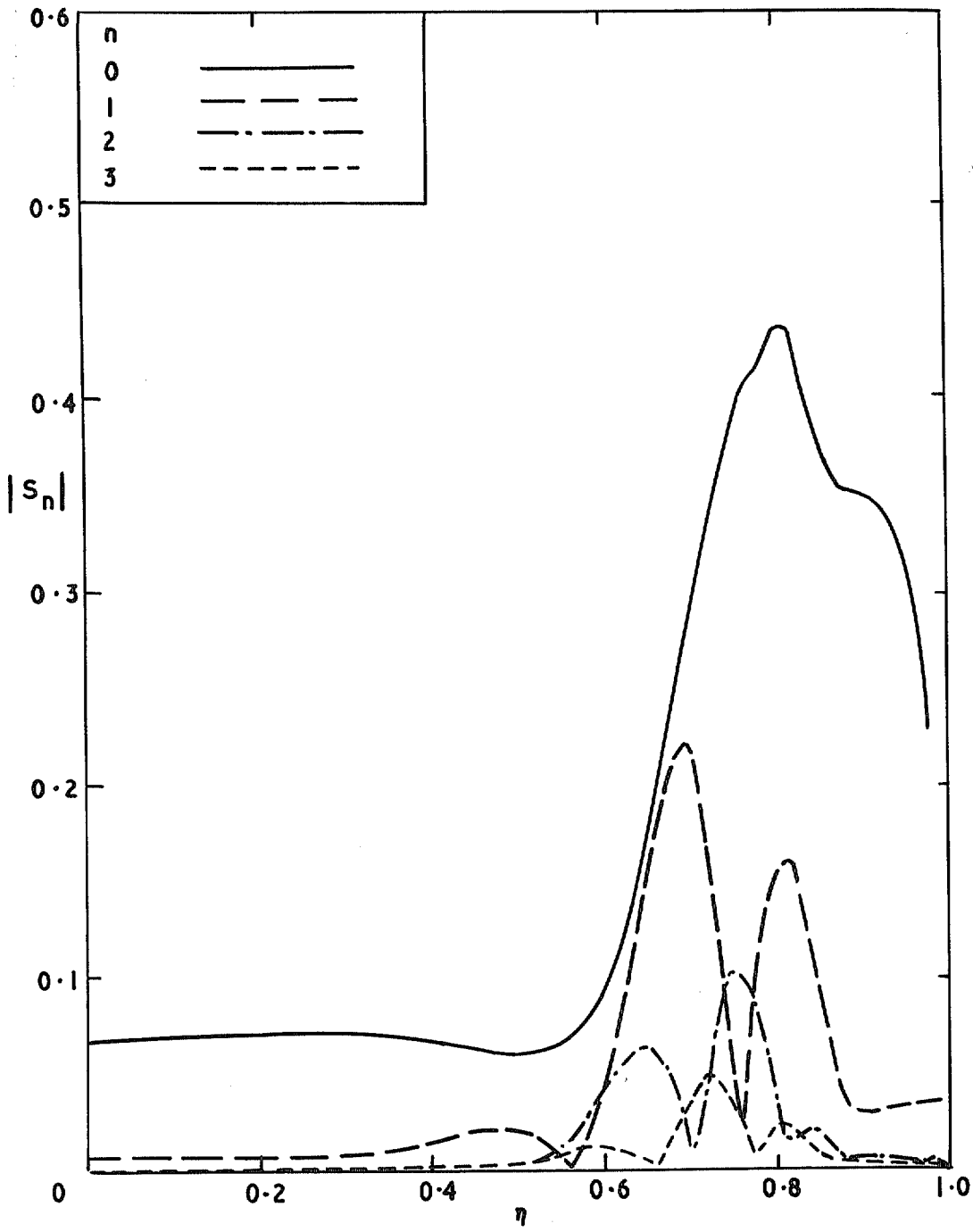

FIG. 21. Spanwise distributions of harmonic components ($|S_n|$) for quasi-steady variation. Station ξ_2, $\bar{\zeta}_0 = 0{\cdot}0262$, $v = 0$, $Re = 2{\cdot}56 \times 10^6$.

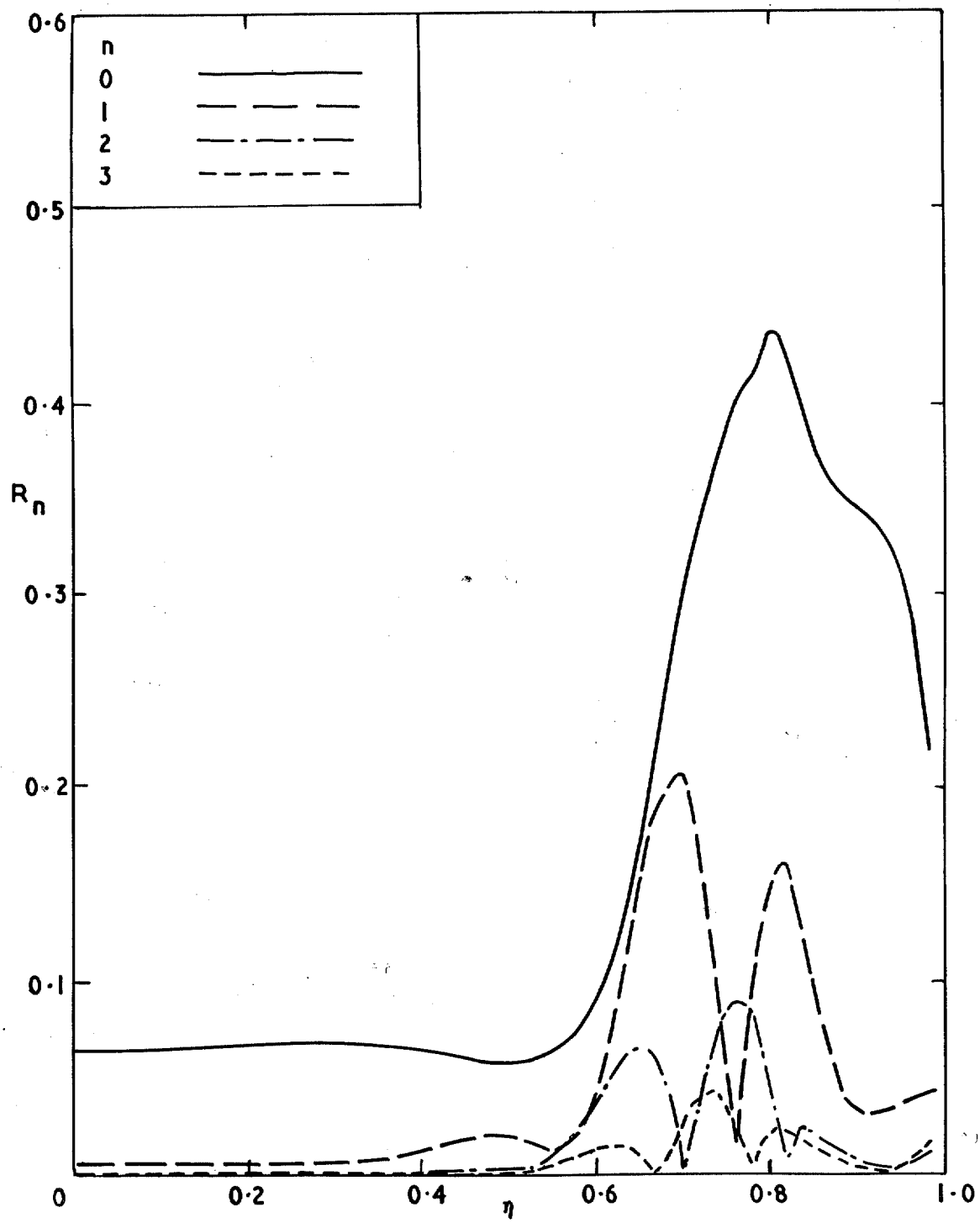

FIG. 22. Spanwise distributions of harmonic components (R_n).
Station ξ_2, $\bar{\zeta}_0 = 0{\cdot}0262$, $v = 1{\cdot}0$, $Re = 2{\cdot}56 \times 10^6$.

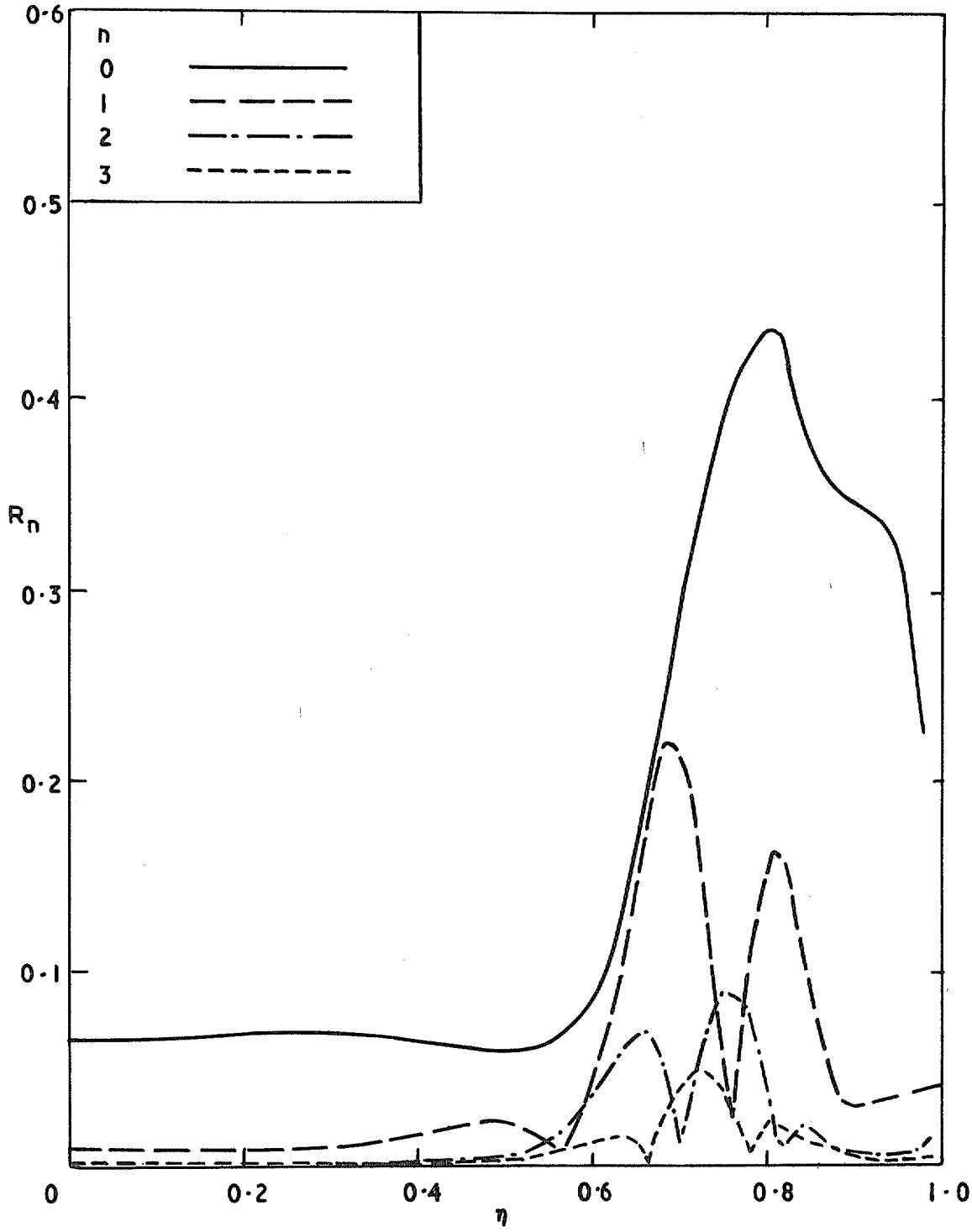

FIG. 23. Spanwise distributions of harmonic components (R_n).
Station ξ_2, $\bar{\zeta}_0 = 0{\cdot}0262$, $v = 0{\cdot}5$, $Re = 2{\cdot}56 \times 10^6$.

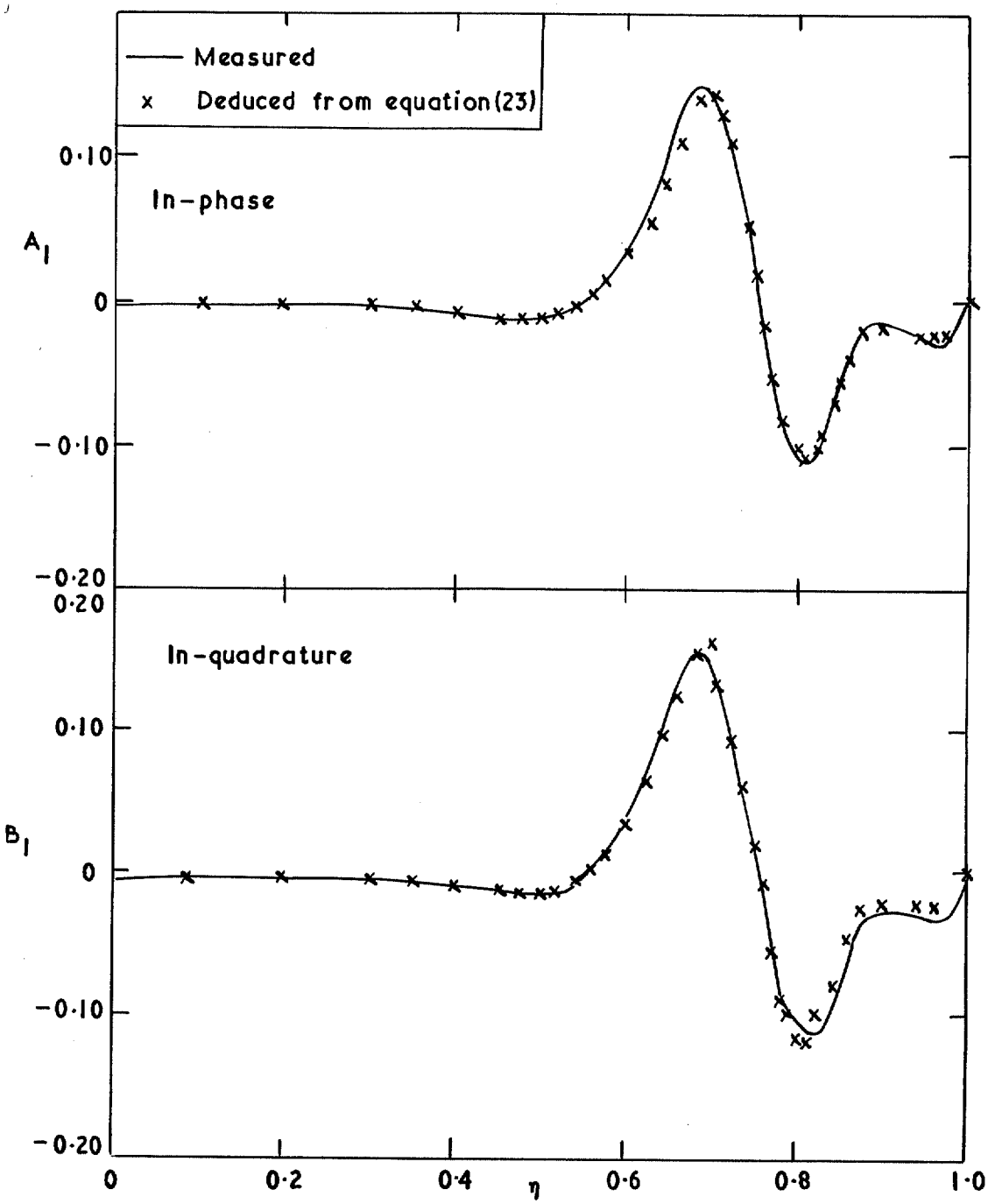

FIG. 26. Spanwise distributions of harmonic components A_1, B_1.
Station ξ_2, $\bar{\zeta}_0 = 0{\cdot}0262$, $v = 1{\cdot}0$, $Re = 2{\cdot}56 \times 10^6$.

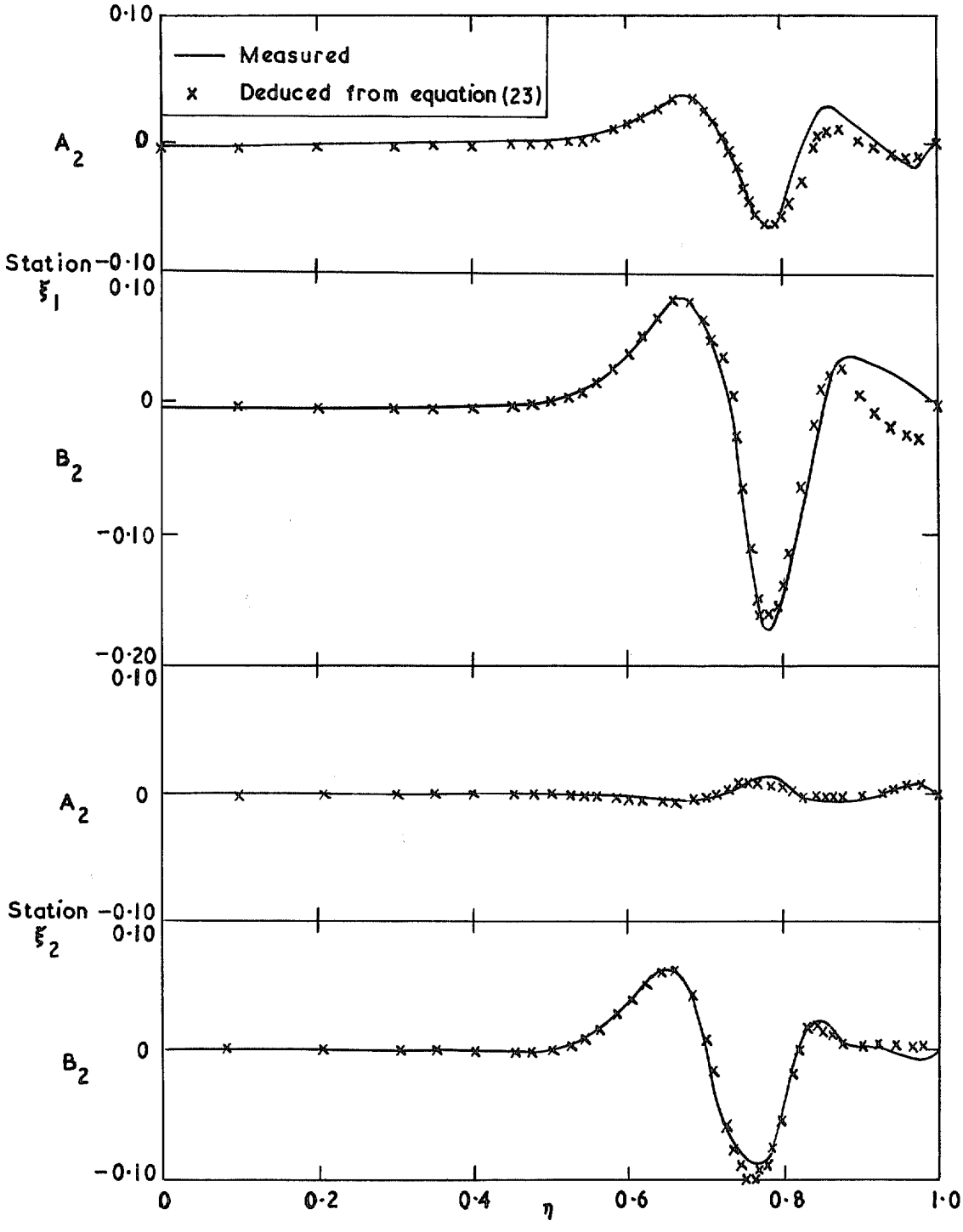

FIG. 27. Spanwise distributions of harmonic components A_2, B_2.
Stations ξ_1, ξ_2, $\bar{\zeta}_0 = 0{\cdot}0262$, $v = 1{\cdot}0$, $Re = 2{\cdot}56 \times 10^6$.

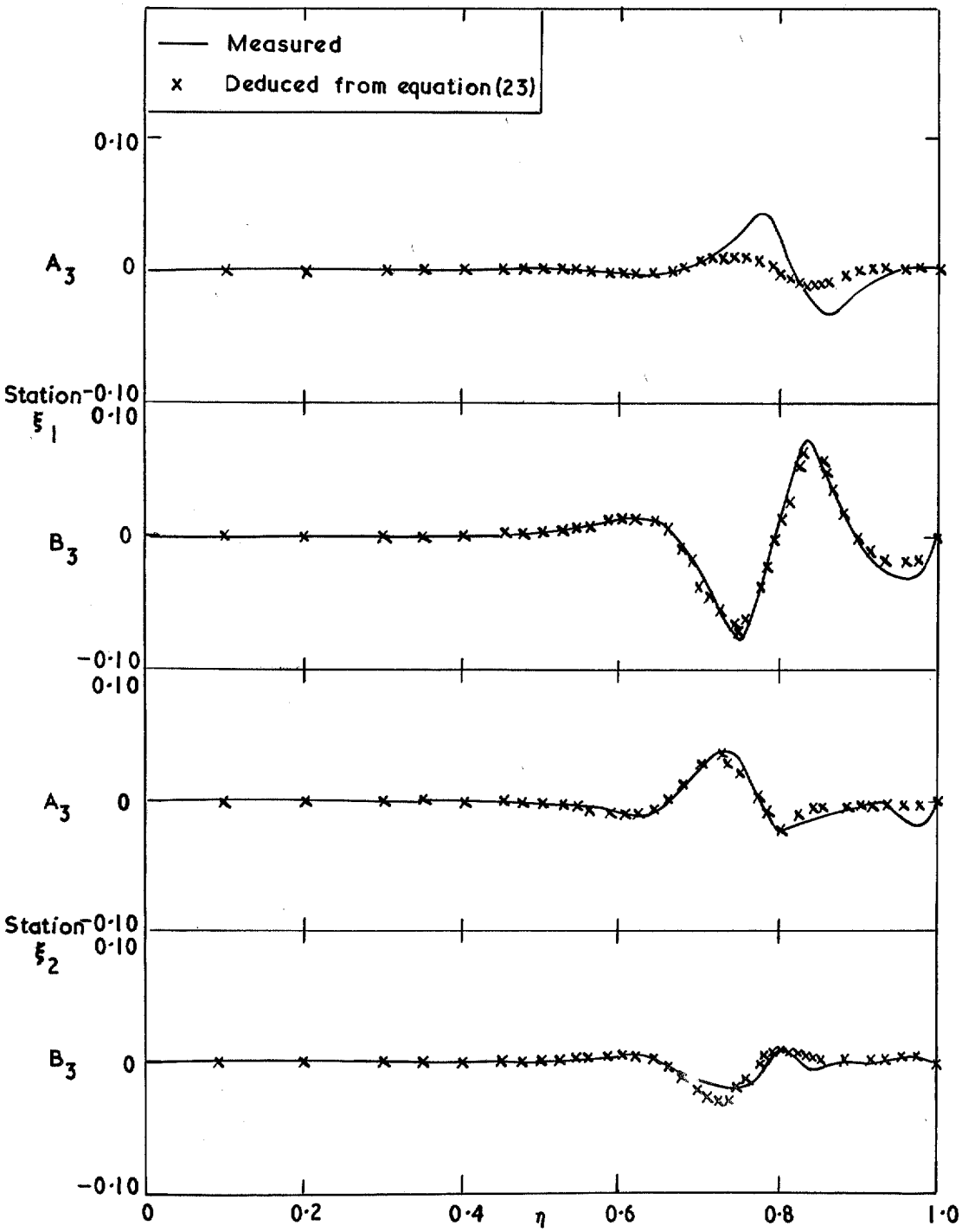

FIG. 28. Spanwise distributions of harmonic components A_3, B_3.
Stations ξ_1, ξ_2, $\bar{\zeta}_0 = 0{\cdot}0262$, $v = 1{\cdot}0$, $Re = 2{\cdot}56 \times 10^6$.

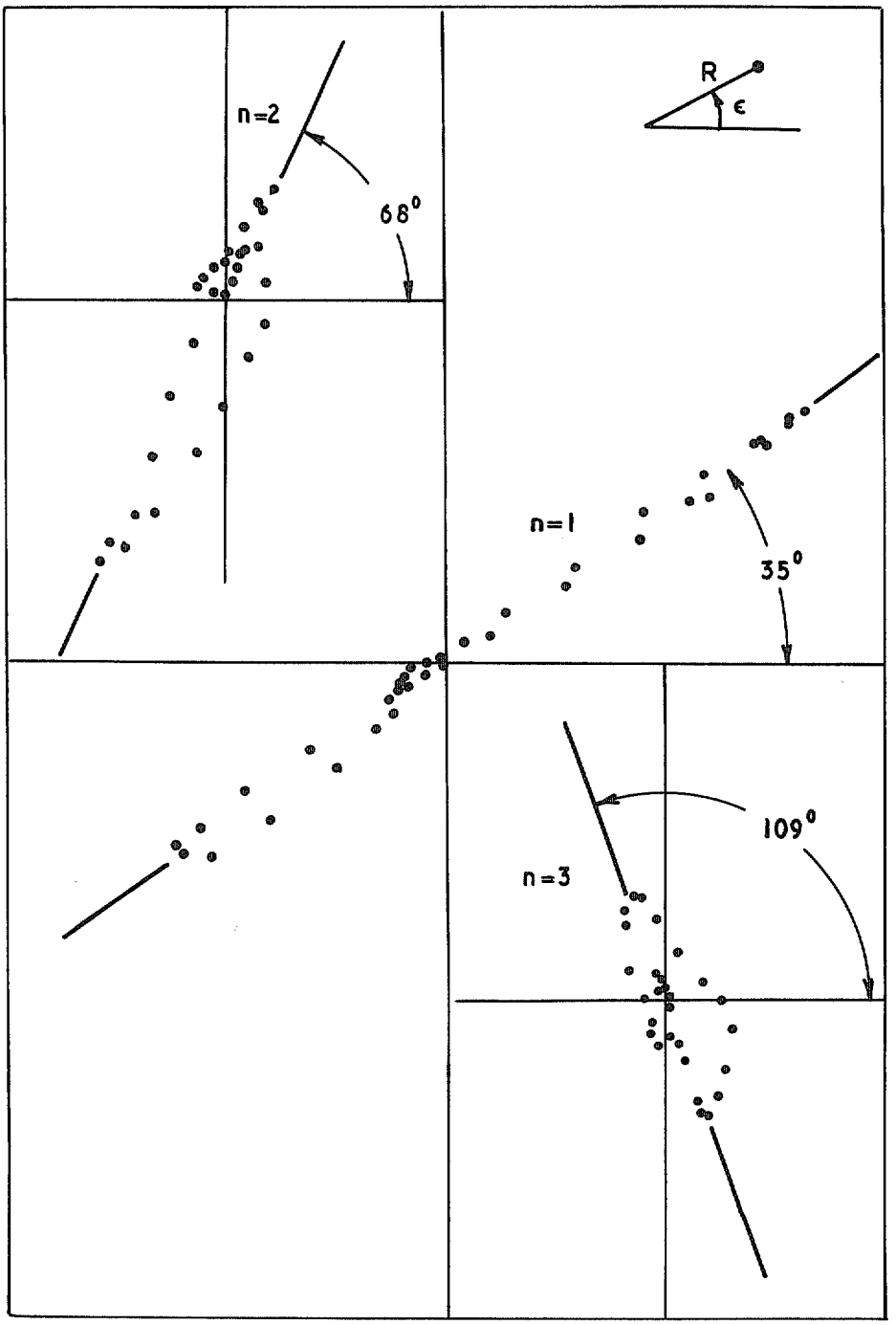

FIG. 29. Polar diagrams of (R, ε) for various spanwise positions $(0<\eta<1{\cdot}0)$. Station ξ_1, $\bar{\zeta}_0=0{\cdot}0262$, $v=1{\cdot}0$, $Re=2{\cdot}56\times10^6$.

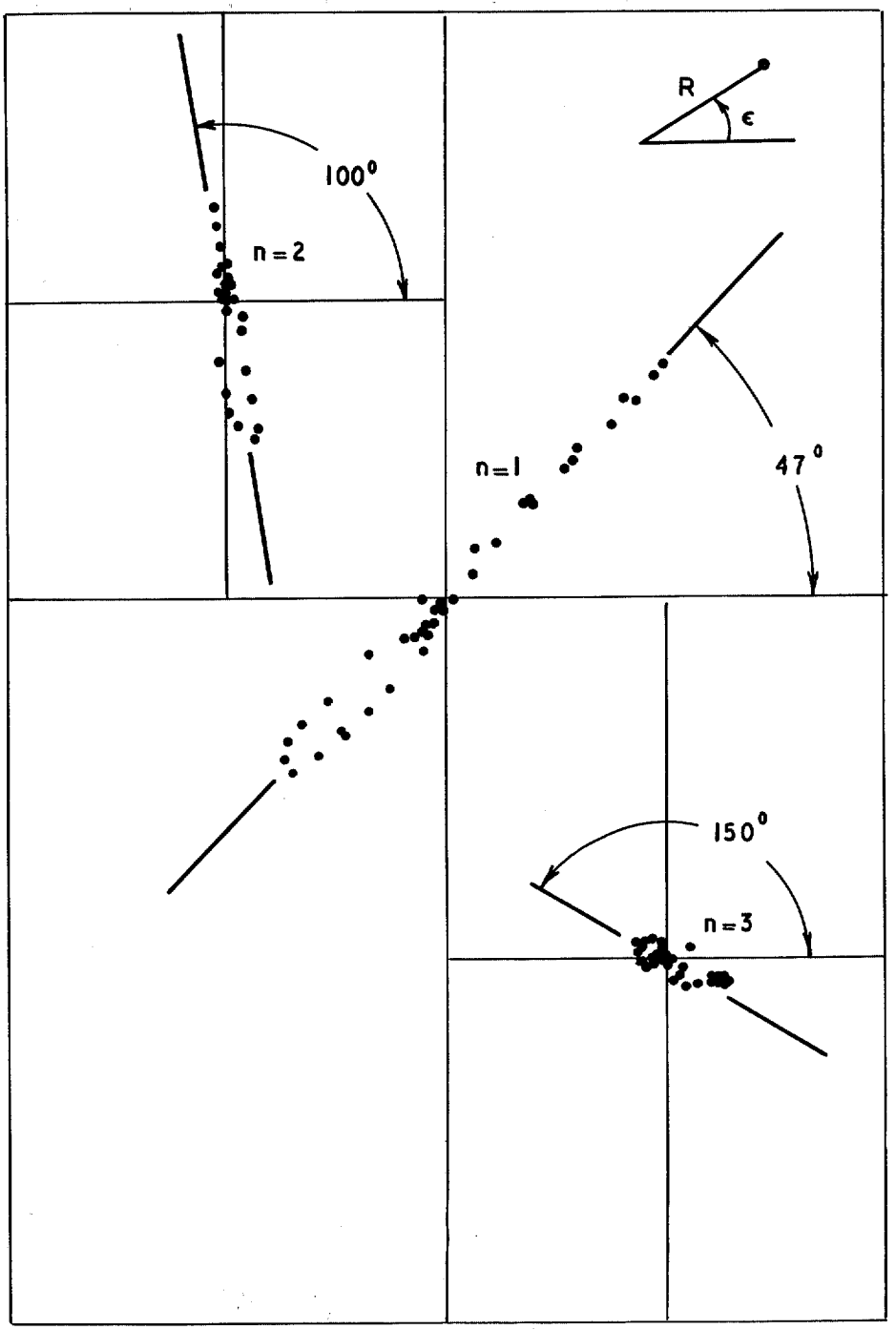

FIG. 30. Polar diagrams of (R, ε) for various spanwise positions $(0<\eta<1{\cdot}0)$. Station ξ_2, $\bar{\zeta}_0=0{\cdot}0262$, $v=1{\cdot}0$, $Re=2{\cdot}56\times10^6$.

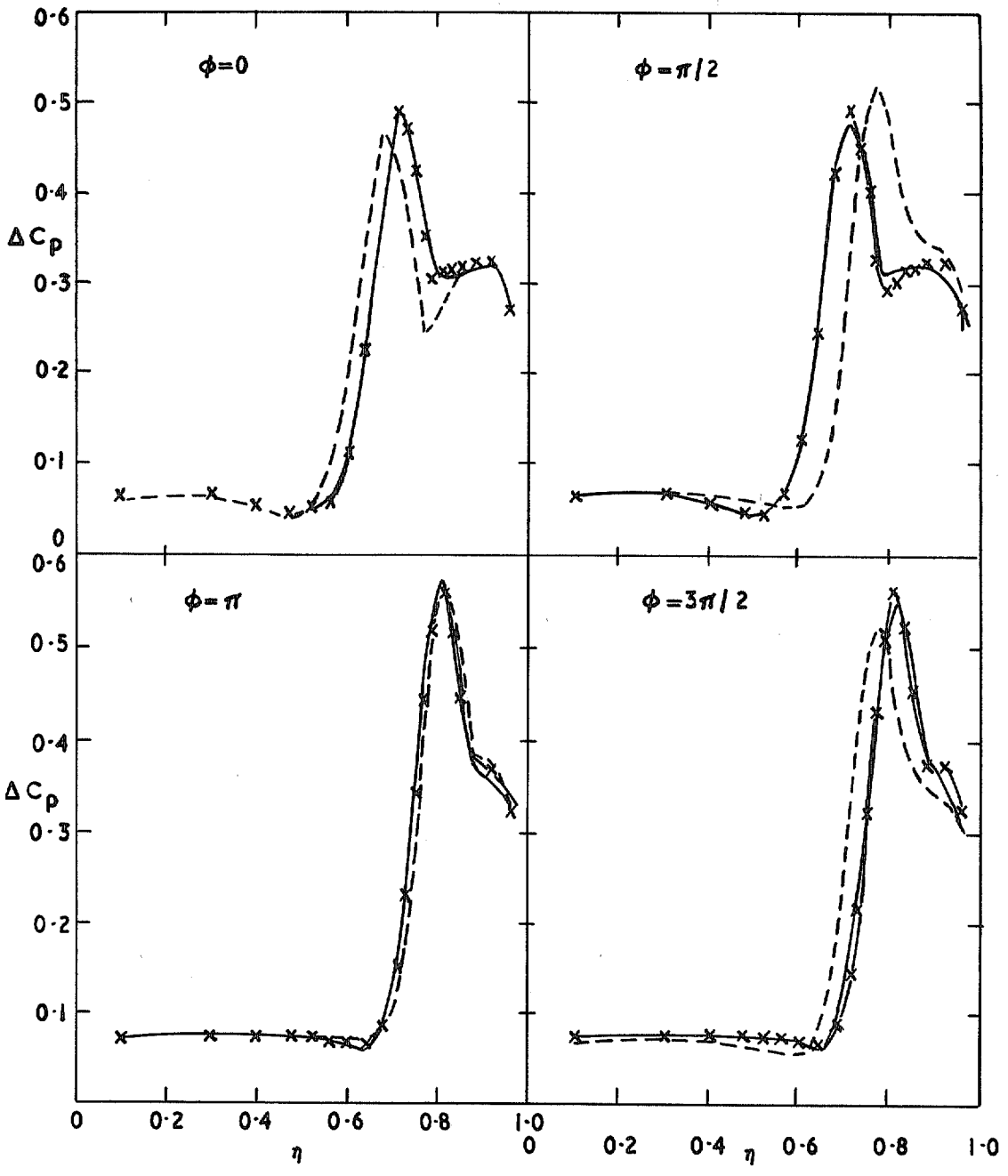

FIG. 31. Instantaneous spanwise pressure distributions.
Station ξ_2, $\bar{\zeta}_0 = 0{\cdot}0262$, $Re = 2{\cdot}56 \times 10^6$.

——— Oscillatory measurements } $v = 1{\cdot}0$
x Deduced using equation (22) }
– – – – – Steady measurements ($v = 0$).

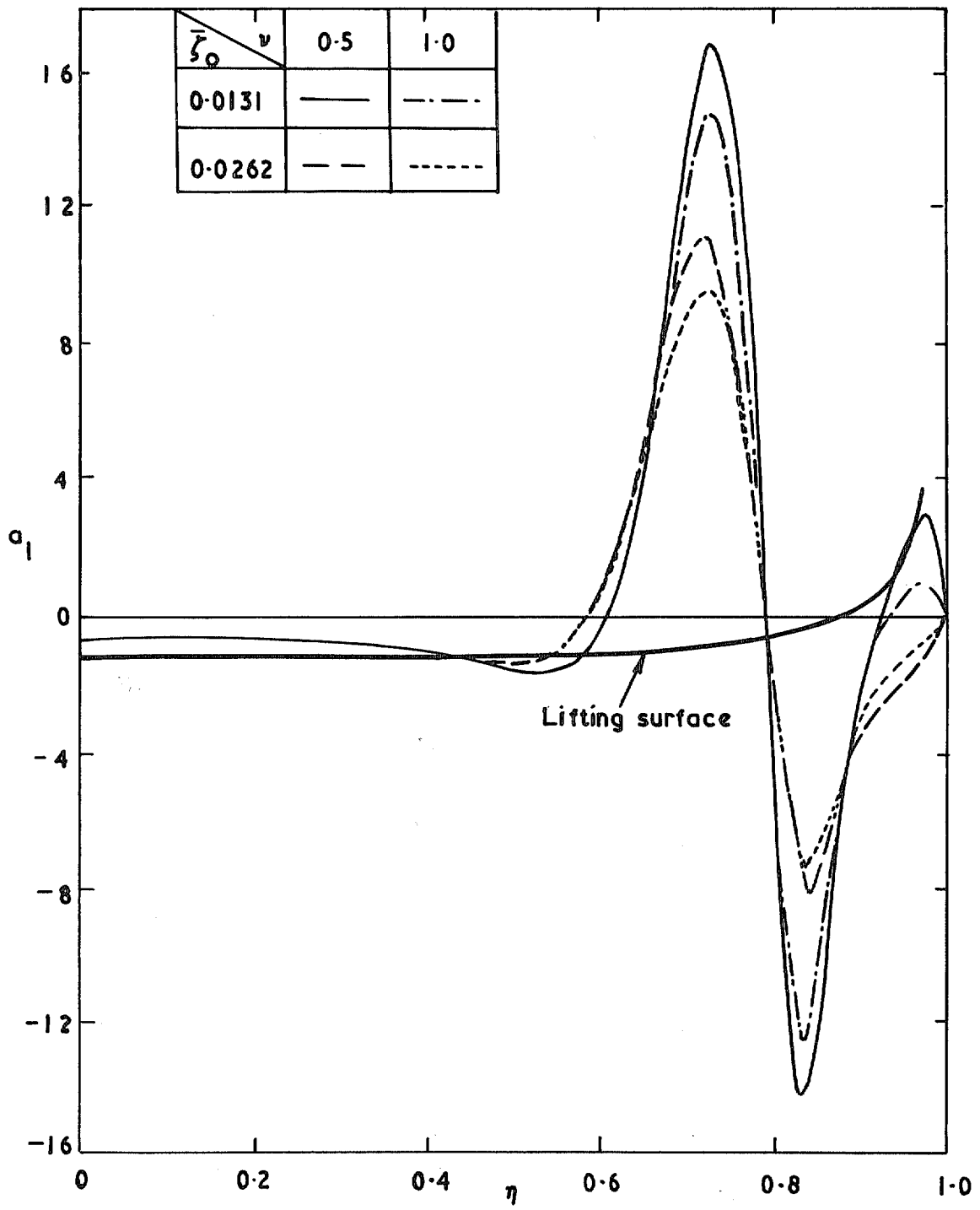

FIG. 32. Spanwise distribution of normalised fundamental components (a_1).
Station ξ_1 $Re = 2{\cdot}56 \times 10^6$.

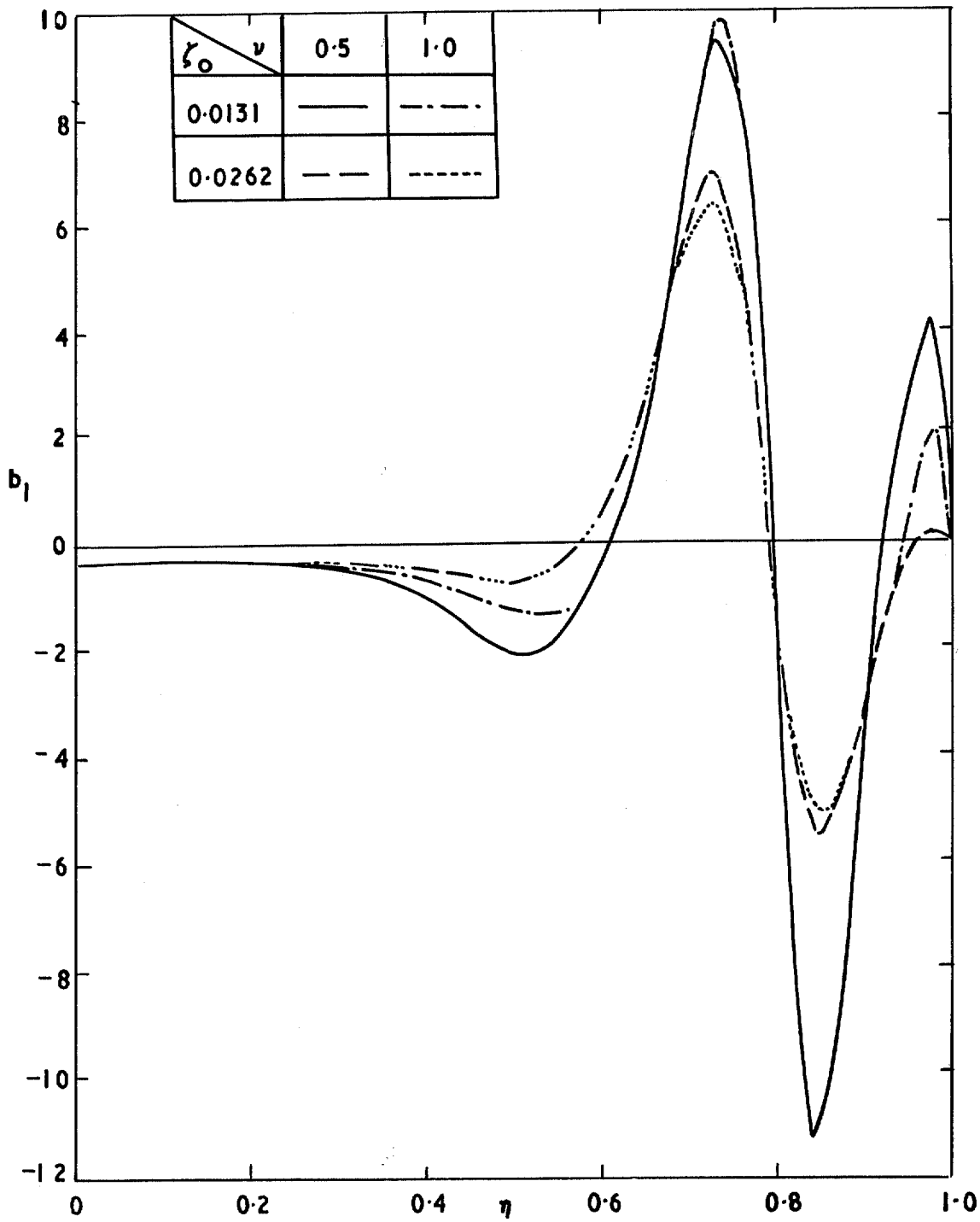

FIG. 33. Spanwise distribution of normalised fundamental components (b_1).
Station ξ_1 $Re = 2{\cdot}56 \times 10^6$.

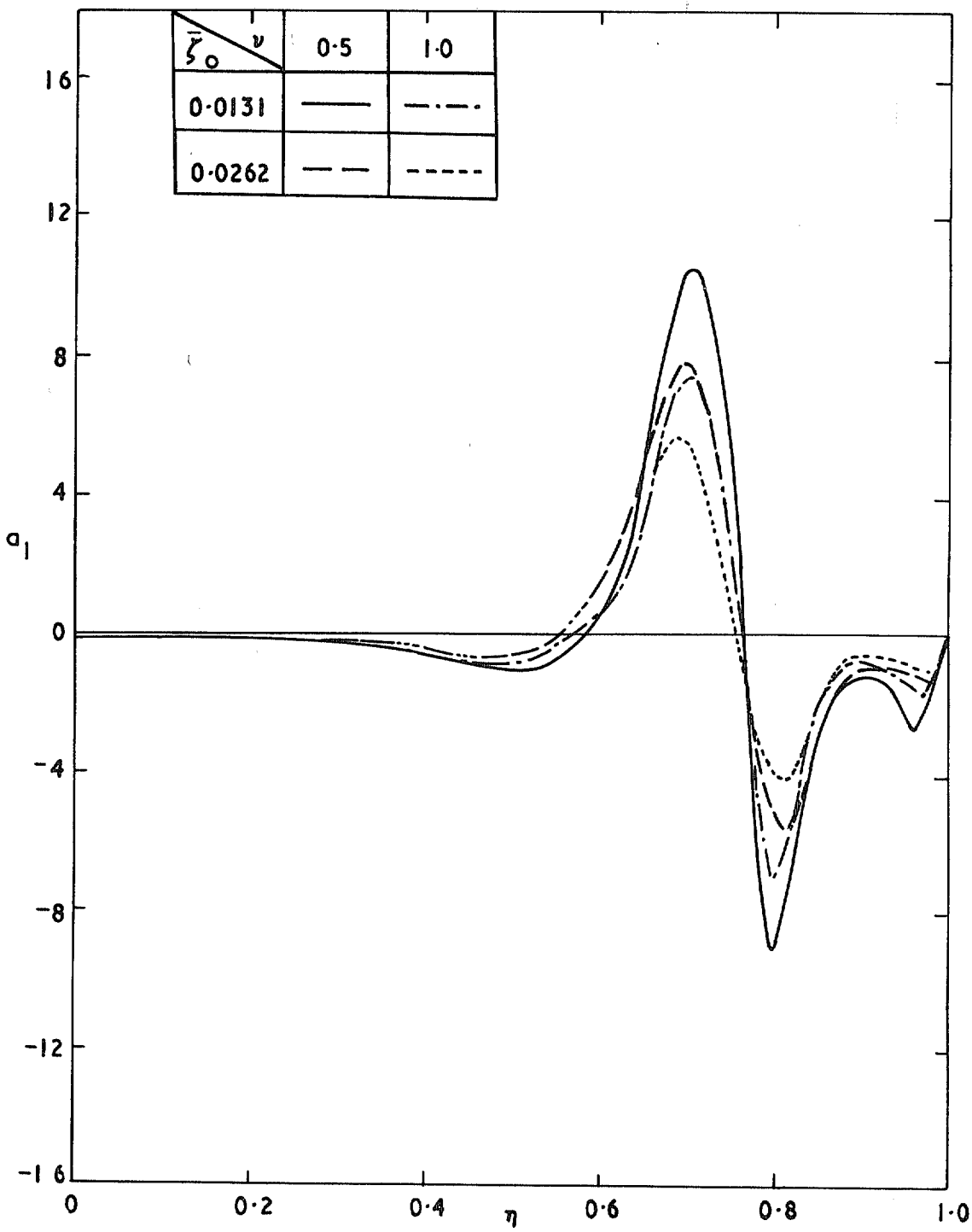

FIG. 34. Spanwise distribution of normalised fundamental components (a_1).
Station ξ_2 $Re = 2{\cdot}56 \times 10^6$.

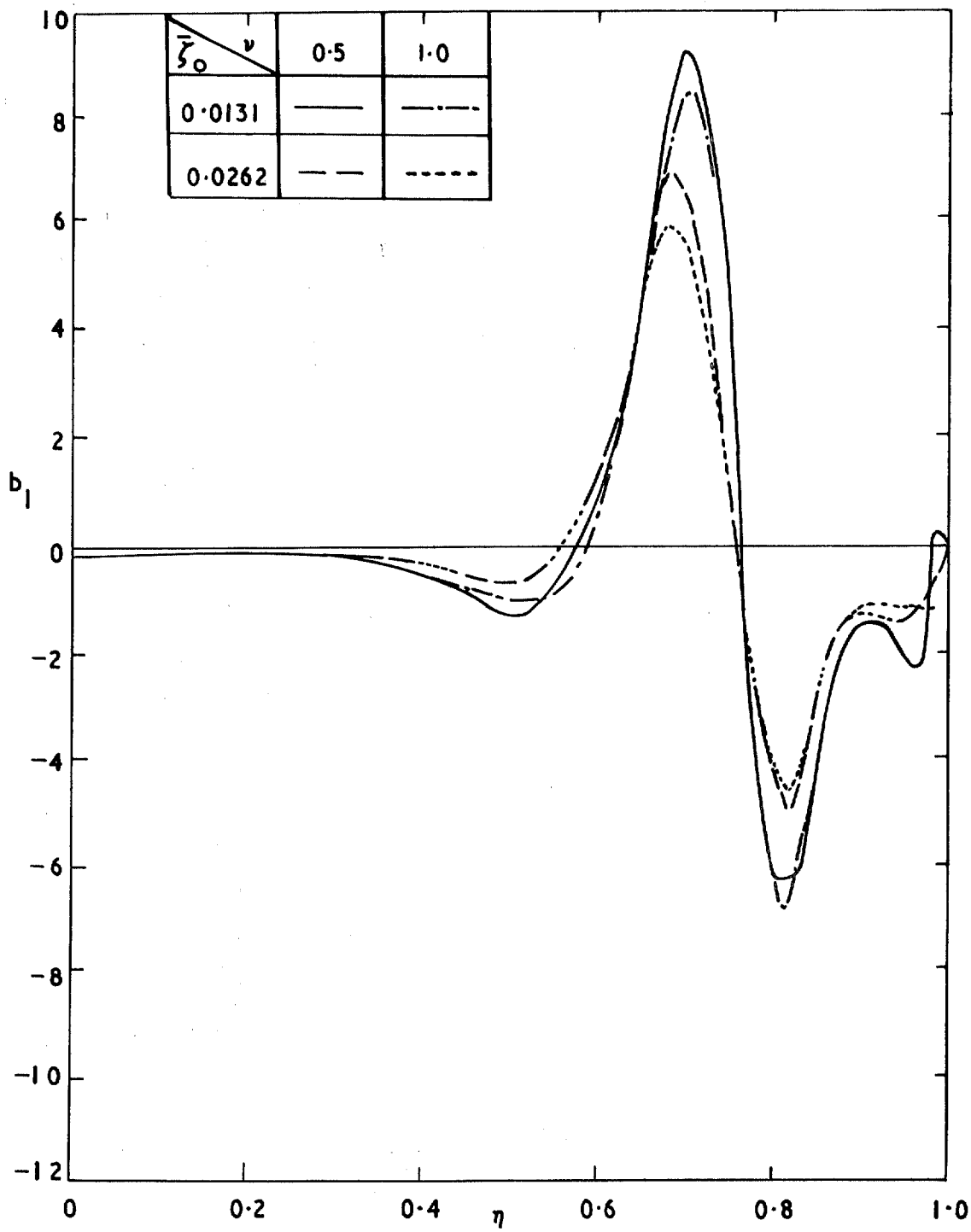

FIG. 35. Spanwise distribution of normalised fundamental components (b_1).
Station ξ_2 $Re = 2{\cdot}56 \times 10^6$.

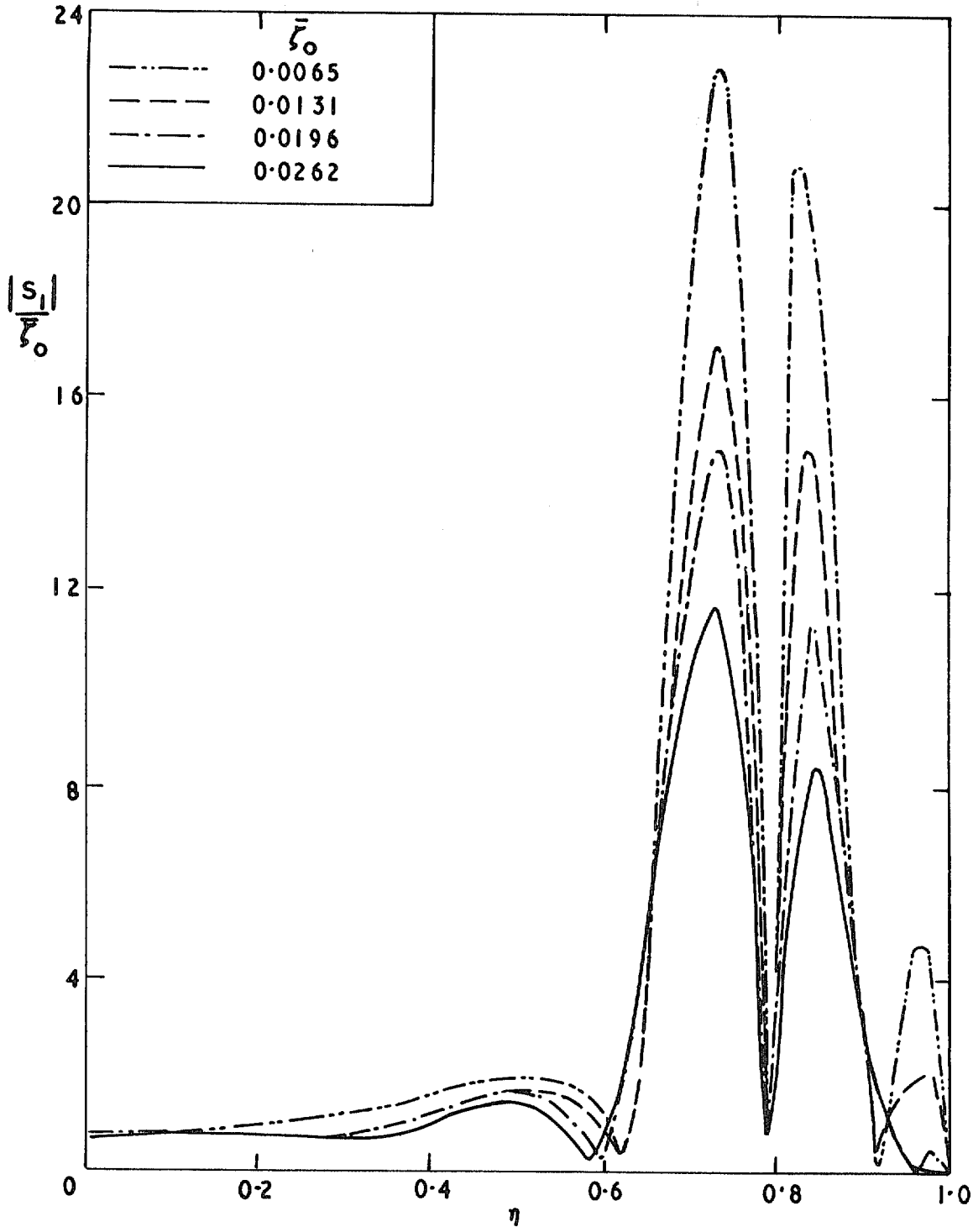

FIG. 36. Spanwise distribution of normalised fundamental amplitude for various values of $\bar{\zeta}_0$.
Station ξ_1, $v=0$ $\quad Re=2{\cdot}56\times10^6$.

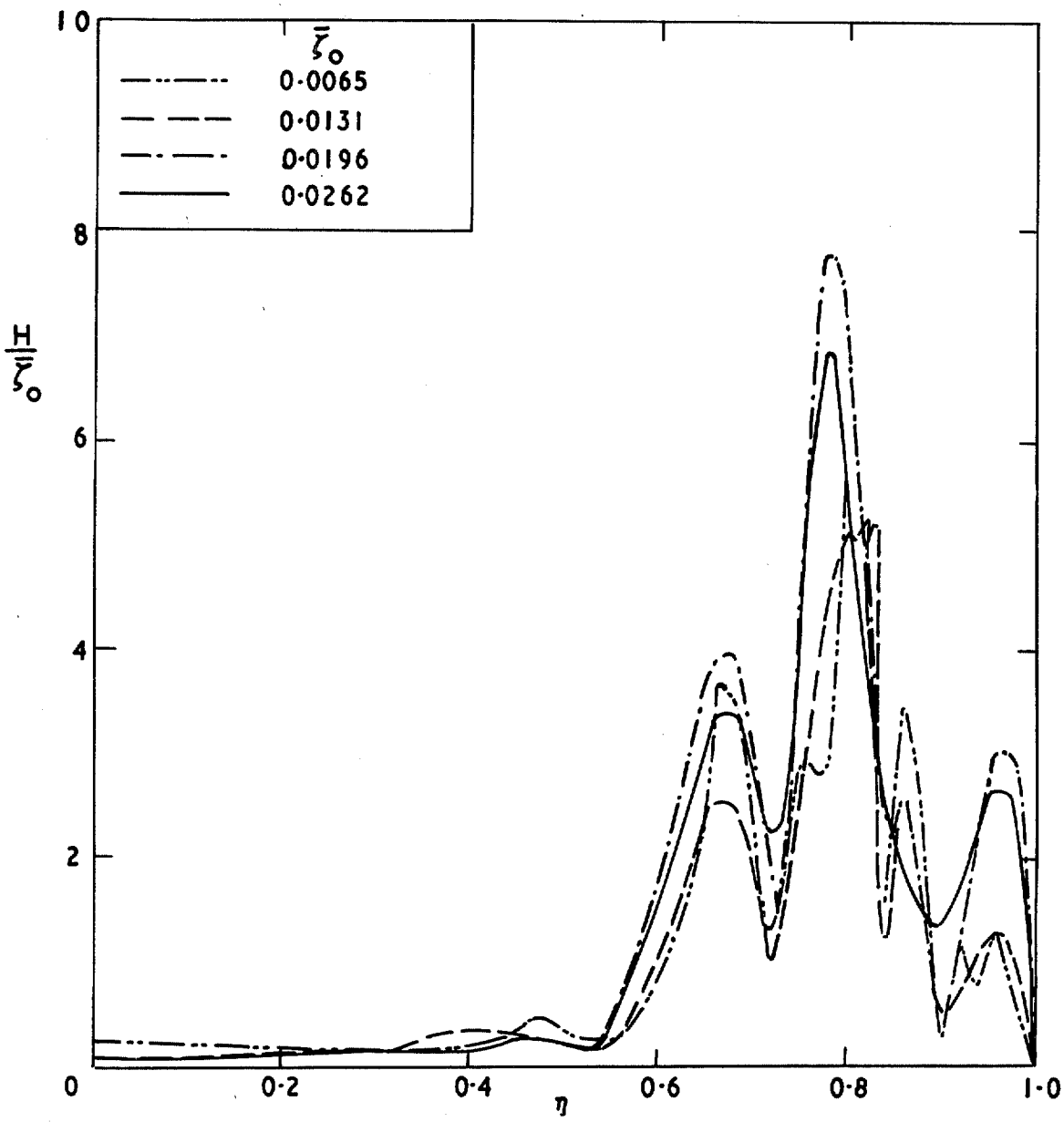

FIG. 37. Spanwise distribution of normalised higher harmonic content for various values of $\bar{\zeta}_0$. Station ξ_1, $v=0$, $Re=2{\cdot}56\times10^6$.

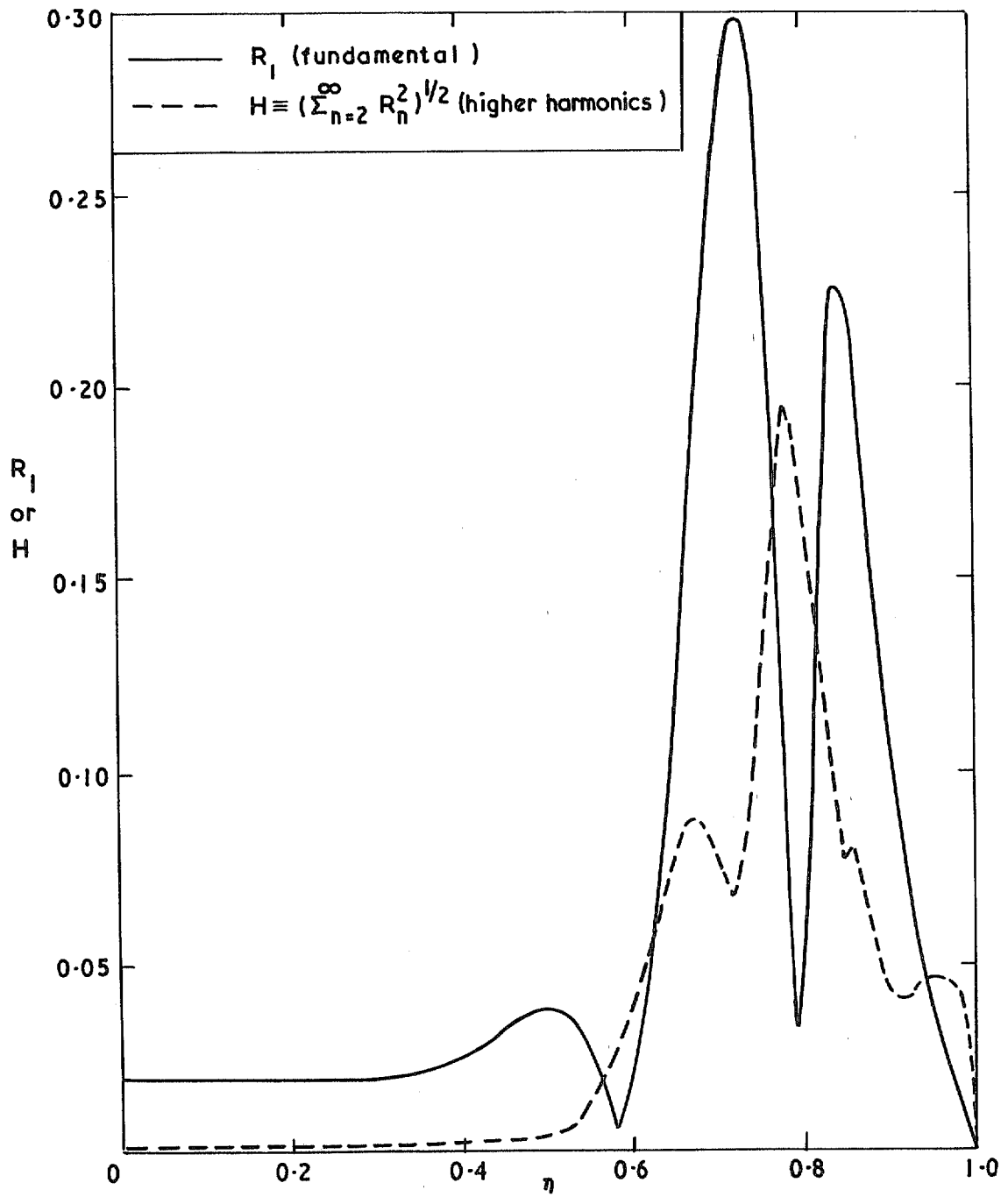

FIG. 38. Spanwise distribution showing comparison between fundamental and higher harmonic components.
Station ξ_1, $v=1{\cdot}0$, $\bar{\zeta}_0=0{\cdot}0262$, $Re=2{\cdot}56\times10^6$.

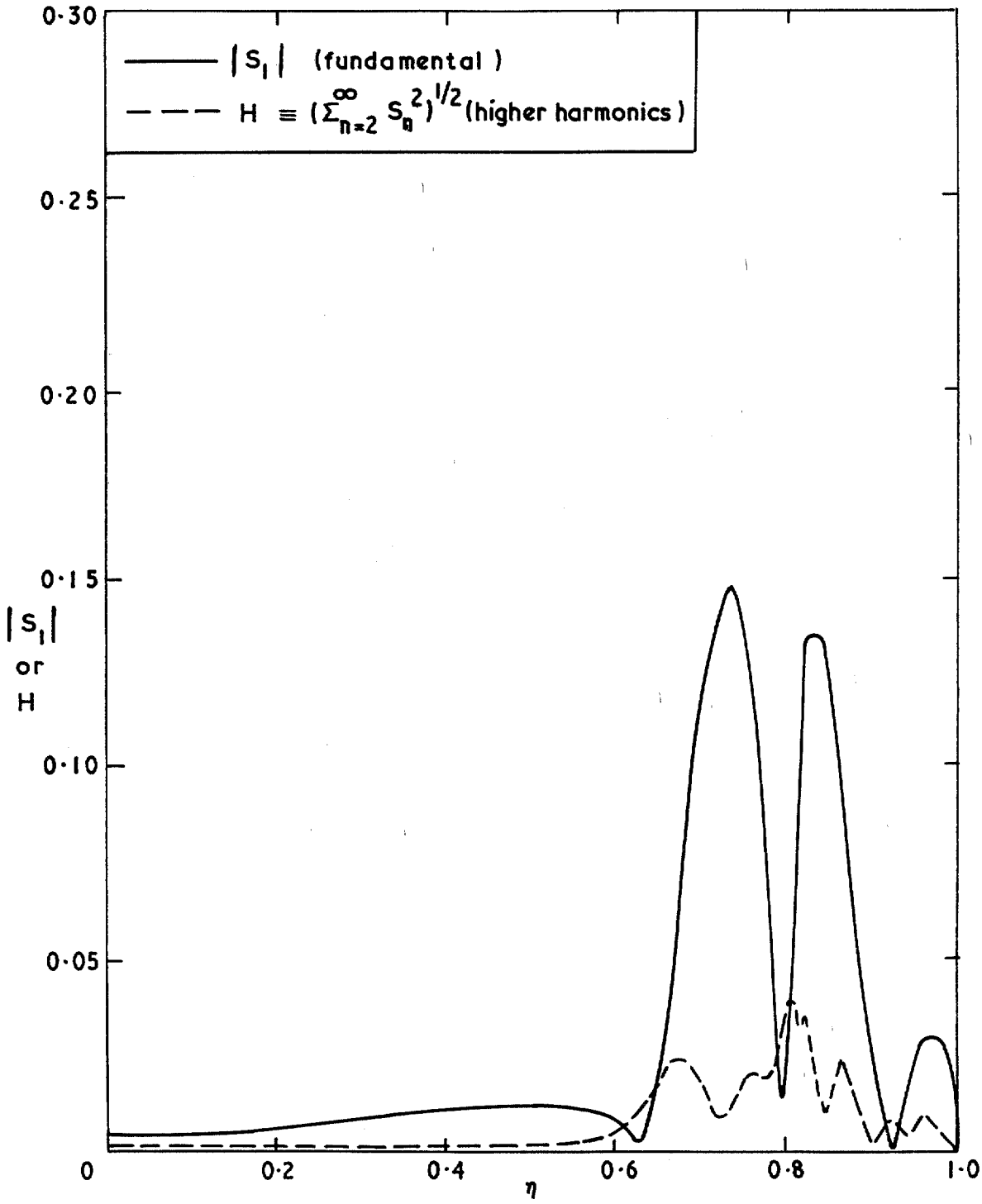

FIG. 39. Spanwise distribution showing comparison between fundamental and higher harmonic components for a quasi-steady variation.
Station ξ_1, $v=0$, $\bar{\zeta}_0=0{\cdot}0065$, $Re=2{\cdot}56\times10^6$.

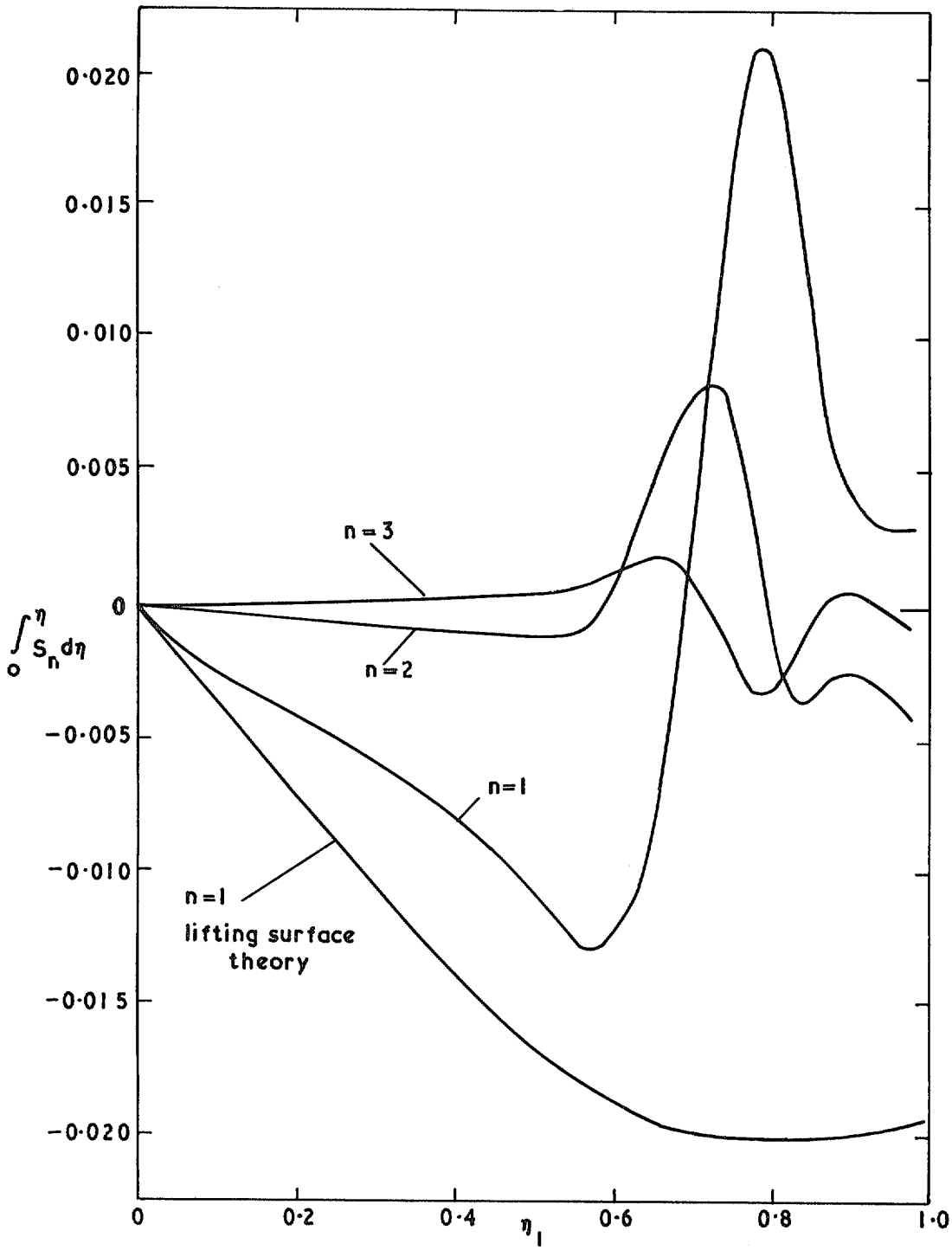

FIG. 40. $\int_0^{\eta_1} S_n d\eta$ plotted against η_1. Station ξ_1, $\bar{\zeta}_0 = 0{\cdot}0262$, $v = 0$, $Re = 2{\cdot}56 \times 10^6$.

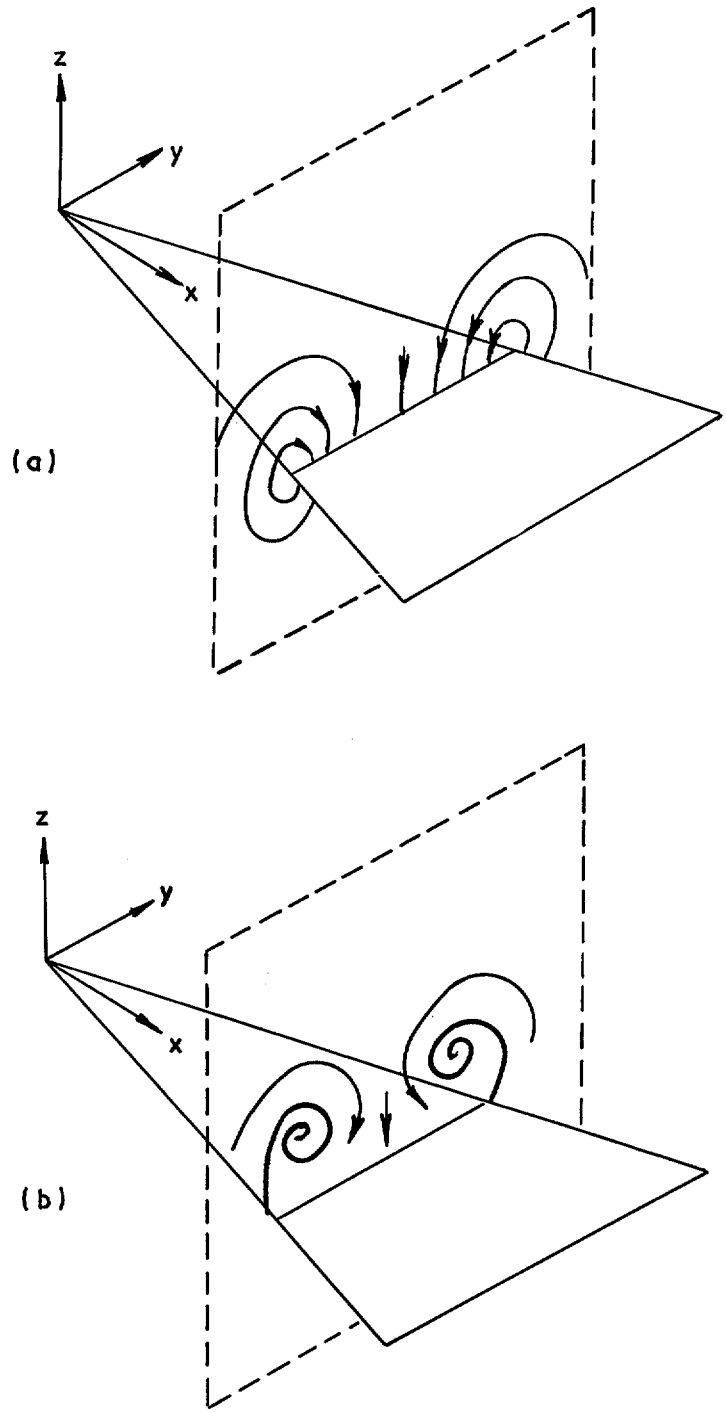

FIG. 41. Cross flow in travelling fluid plane (a) Irrotational flow (b) Separated flow.

Printed in Wales for Her Majesty's Stationery Office by Allens Printers (Wales) Limited
Dd. 502110 K.5.

Published by
HER MAJESTY'S STATIONERY OFFICE

To be purchased from
49 High Holborn, London WC1V 6HB
13a Castle Street, Edinburgh EH2 3AR
109 St Mary Street, Cardiff CF1 1JW
Brazennose Street, Manchester M60 8AS
50 Fairfax Street, Bristol BS1 3DE
258 Broad Street, Birmingham B1 2HE
80 Chichester Street, Belfast BT1 4JY
or through booksellers

SBN 11 470493 7